

ESTIMATION OF BASIN DETECTION AND REPRESENTATION FROM
NON-LINEAR SYSTEM DATA

By

Mehmet Gökhan Habiboğlu

B.S., Electrical and Electronic Engineering, Boğaziçi University, 2004

Submitted to the Institute for Graduate Studies in
Science and Engineering in partial fulfillment of
the requirements for the degree of
Master of Science

Graduate Program in Electrical and Electronic Engineering
Boğaziçi University

2007

ESTIMATION OF BASIN DETECTION AND REPRESENTATION FROM
NON-LINEAR SYSTEM DATA

APPROVED BY:

Assoc. Prof. Yağmur Denizhan
(Thesis Supervisor)

Prof. Yorgo İstefanopulos

Assist. Prof. Murat Saraçlar

DATE OF APPROVAL: 15.06.2007

ABSTRACT

ESTIMATION OF BASIN DETECTION AND REPRESENTATION FROM NON-LINEAR SYSTEM DATA

In this thesis, we are interested in a good qualitative representation of a nonlinear autonomous flow. It is assumed that the equations governing a given nonchaotic nonlinear autonomous flow are unknown. The only prior knowledge about the system is its dimension, that is to say the number of state variables. As a realistic assumption this analysis will be confined to a part of the state space where the initial conditions are gathered. On the basis of a set of trajectory recordings gathered for a sufficiently large set of initial conditions our task is to identify the possible long term behaviour alternatives and to determine the set of initial conditions starting from which the system trajectories exhibit a specified long term behaviour.

We will use different mathematical tools such as kernel estimation algorithms or image processing filters to visualize the long term behaviour of the given system. After the geometrical identification of important characteristic behaviours in our nonlinear system, we will define the basin of attractions and basins of some other phenomena with the help of algorithms which are originally developed. Proposed algorithms will be used first on two dimensional non-linear phase portraits and then will be extended to the third dimension with restrictions and limitations. Chaotic systems will be omitted due to their complicated strange attractor phenomena.

Multivariate kernel estimators will be used among many places in the thesis. We will restrict ourself to diagonal bandwidth matrices since the optimal multivariate kernel estimators, especially if the system bandwidth varies according to the data position, are too complicated to find a place in this study.

These estimation techniques and our algorithmic contribution will give a better insight about the long term behaviour of non-linear systems and will help us accomplish the aim of the thesis which is to identify the attractors of a continuous time, autonomous, non-chaotic system and to provide an approximate description of the basins of attractions to be used later for control purposes.

ÖZET

DOĞRUSAL OLMAYAN SİSTEM VERİSİNDEN HAVZA SEZİMİ VE TEMSİLİNİN KESTİRİMİ

Bu tezde, doğrusal olmayan özerk akışların nitel bir temsilini çıkarmaya çalıştık. Kaotik ve doğrusal olmayan özerk akışları yöneten denklemlerin bilinmediği ve sistem hakkında önceden bilinen tek bilginin sistemin boyutu olduğu varsayıldı. İncelememizi yalnızca durum uzayında başlangıç koşullarının toplandığı bölgelerden yaptık. Görevimiz, yeterince çok sayıda başlangıç koşulundan kaydolunmuş bir grup gezingeyi temel alarak, sistemin mümkün olan tüm uzun dönem davranış biçimlerini tanımlamak ve sistem gezinelerinin hangi başlangıç koşullarından başladığında hangi davranış biçimini sergileyeceğini belirlemektir.

Tez boyunca “çekirdek kestirimi” veya “imge işleme filtreleri” gibi farklı matematiksel araçlar kullanıldı. Doğrusal olmayan sistemlerdeki önemli karakteristik davranışlar geometrik olarak tanımlandıktan sonra, çekim havzaları ve diğer bazı havza türleri kendi geliştirdiğimiz algoritmaların yardımlarıyla tanımlandı. Önerilen algoritmalar önce iki boyutlu faz portrelerinde kullanıldı, daha sonra da bazı kısıtlarla üç boyutlu sistemlere genişletildi. Kaotik sistemler, komplike garip çekici fenomenleri yüzünden teze dahil edilmedi.

Çok değişkenli çekirdek kestiricileri tez boyunca bir çok yerde kullanıldı. Ancak yalnızca bant genişliği köşegen matrislerden oluşan kestiriciler kullanıldı. Bunun nedeni en iyi çok değişkenli çekirdek kestiricilerin bulunmasının, özellikle de bant genişliği verinin yerine göre değişiyorsa, bu tezde araştırmak için çok komplike olmasıdır.

Bu kestirim teknikleri ve algoritmik katkı, sürekli, otomatik, kaotik olmayan ve doğrusal olmayan sistemlerin uzun dönem davranışları hakkında bize hem daha iyi bir anlayış sağladı, hem de bu sistemlerin çekicilerini belirleme konusunda ve daha sonra kontrol amaçlı kullanılacak bu çekicilerin havzaları üzerine yaklaşık bir tanımlama verme konusunda yardımcı oldu.

TABLE OF CONTENTS

	Page
ABSTRACT.....	iii
ÖZET.....	iv
LIST OF FIGURES.....	vii
1. INTRODUCTION.....	1
1.1. Dynamical Systems.....	1
1.2. Nonlinear Systems.....	1
1.3. Regression Types.....	3
2. MATHEMATICAL BACKGROUND.....	6
2.1. Analysis of Non-Linear Dynamical Systems.....	6
2.1.1 Two Dimensional Systems.....	7
2.1.2 Phase Plane Analysis in Linear Systems.....	7
2.1.3 Phase Plane Analysis in Non-Linear Systems.....	10
2.1.4 Limit Cycle.....	12
2.2. Regression Models and Kernel Estimators.....	13
2.2.1 Histograms and Univariate Kernel Estimator.....	13
2.2.2 Multivariate Kernel Estimation.....	21
2.2.3 Parametric Regression.....	25
3. METHODOLOGY.....	28
3.1. Identification of Stable Equilibrium Points.....	28
3.2. Identification of Periodic Orbits and Limit Cycles.....	31
3.3. Identification of Exit Boundary Segments.....	37

3.4. Flame Expansion Algorithm.....	39
4. COMPLEMENTARY WORK AND DIFFERENT APPROACHES.....	44
4.1. Image Processing Filters	44
4.2. The Backbone Extraction	49
4.3. Preliminary Work for 3-Dimensional Systems	51
5. SIMULATION RESULTS	57
5.1. System I.....	58
5.2. System II	63
5.3. System III	66
5.4. System IV	71
5.5. System V	76
5.6. Data Point Test	80
6. DISCUSSION AND CONCLUSION	81
6.1. Limitations.....	81
6.2. Future Work.....	83
REFERENCES.....	85

LIST OF FIGURES

		Page
Figure 2.1	Limit Cycle.....	13
Figure 2.2	40 Random Numbers between 0-1.....	15
Figure 2.3	Histograms with Different Starting Points	16
Figure 2.4	Histograms with Different Bandwidths	16
Figure 2.5	Trajectory for Logistic Map	19
Figure 2.6	Oversmoothed Estimate	20
Figure 2.7	Undersmoothed Estimate	20
Figure 2.8	Optimum Estimate	21
Figure 2.9	Density Example and 2D Kernel Function	24
Figure 2.10	Sample of Data Points.....	26
Figure 2.11	Estimation of the Boundary with 3. Model	27
Figure 2.12	Estimation of the Boundary with 4. Model	27
Figure 3.1	Phase Portrait of the 2D-Example	29
Figure 3.2	Equilibrium Point Candidates.....	30
Figure 3.3	Kernel Regression of Equilibrium Point Candidates	30
Figure 3.4	Poincare Line	32
Figure 3.5	Poincare Line on Periodic Orbit	32
Figure 3.6	Intersection Points of Poincare Line	33
Figure 3.7	Sampled Continuum of Periodic Orbits	34
Figure 3.8	Phase Portrait of a System with a Limit Cycle.....	35
Figure 3.9	Limit Cycle in the Phase Portrait.....	35
Figure 3.10	Limit Cycle Stability Analysis.....	36

Figure 3.11	Phase Portrait Example for Exit Boundary Identification.....	37
Figure 3.12	Exit Boundary Points	38
Figure 3.13	Kernel Regression of Exit Boundary Points.....	39
Figure 3.14	Three Different Kind of Flames.....	40
Figure 3.15	Expansion of the Flames after 1 Iteration	41
Figure 3.16	Expansion of the Flames after 2 Iterations	41
Figure 3.17	Expansion of the Flames after 6 Iterations	42
Figure 3.18	Expansion of the Flames after 10 Iterations	42
Figure 3.19	Expansion of the Flames after 22 Iterations	43
Figure 4.1	Effect of the Sharpening Filter	45
Figure 4.2	Choosing the Neighbour Points	47
Figure 4.3	Phase Portrait after Filtering.....	48
Figure 4.4	Backbones.....	50
Figure 4.5	Backbone Estimation from the Activated Peaks d.....	50
Figure 4.6	Phase Portrait of a 3D-System.....	51
Figure 4.7	Trajectories Entering and Flowing Out.....	52
Figure 4.8	Exit and Entrance Points on ROI.....	53
Figure 4.9	Flame Expansion on Surfaces of ROI.....	54
Figure 4.10	Boundaries on the Surface.....	54
Figure 4.11	Flame Expansion inside the ROI	55
Figure 4.12	Boundary of Basin of Equilibrium Points	56
Figure 5.1	Phase Portrait of System I	58
Figure 5.2	Kernel Regression of Exit Points of System I.....	59
Figure 5.3	Periodic Orbits of System I	59

Figure 5.4	System I after Totally Burnt	60
Figure 5.5	1. Exit Basin Estimation of System I	60
Figure 5.6	2. Exit Boundary Estimation of System I.....	61
Figure 5.7	Periodic Orbit Estimation of System I	62
Figure 5.8	Phase Portrait of System II d	63
Figure 5.9	Kernel Regression of Exit Boundary Points.....	64
Figure 5.10	Kernel Regression of Attractive Equilibrium Points of System II	64
Figure 5.11	System II after Totally Burnt.....	65
Figure 5.12	Border of one of the Exit Basins of System II.....	65
Figure 5.13	Estimation of the Exit Basin of System II.....	66
Figure 5.14	Phase Portrait of System III.....	67
Figure 5.15	Existence of Exit Points of System III	67
Figure 5.16	Kernel Regression of Attractive Equilibrium Points of System III.....	68
Figure 5.17	Existence of Periodic Orbits of System III.....	68
Figure 5.18	Estimation of 1. Basin of Attraction of System III	69
Figure 5.19	Estimation of 2. Basin of Attraction of System III	70
Figure 5.20	Phase Portrait of System IV	71
Figure 5.21	Existence of Exit Points of System IV	72
Figure 5.22	Kernel Regression of Attractive Equilibrium Points of System IV.....	72
Figure 5.23	Existence of Periodic Orbits of System IV	73
Figure 5.24	System IV after Totally Burnt	73
Figure 5.25	Estimation of 1. Basin of Attraction of System IV	74
Figure 5.26	Estimation of 1. Basin of Attraction of System IV via Third Order Polynomial.....	75
Figure 5.27	Phase Portrait of System V	76

Figure 5.28	Kernel Regression of Exit Boundary Points of System V	77
Figure 5.29	Existence of Attractive Equilibrium Points of System V.....	77
Figure 5.30	Limit Cycle of System V.....	78
Figure 5.31	System V after Totally Burnt.....	78
Figure 5.32	Estimation of Basin of Attraction of System V	79

1. INTRODUCTION

1.1. Dynamical Systems

Dynamical systems consist of a set of states, together with a rule that determines the present state in term of past states and possibly an input. In other words, dynamical systems are systems which have memories, they determine the present state according to their past states. So, they are deterministic instead of being random or stochastic.

Dynamical systems can be represented in two forms dependent on their nature:

- differential equations, which define systems in continous time and
- difference equations, which evolve systems in discrete time.

In our thesis, we will research the continous time dynamical system which can be represented as:

$$\dot{\underline{x}}(t) = f(\underline{x}(t)) \quad (1.1)$$

where,

$\dot{\underline{x}}(t)$: n-dimensional vector. we will use \dot{x} instead of $\dot{\underline{x}}(t)$ to simplify the notation.

$f(\underline{x}(t))$: n-dimensional vector field which is a realistic assumption for any real system. Furthermore $f(\underline{x}(t))$ has no explicit dependence on time, that is to say it is an autonomous system. In our thesis, we will refer to such dynamics as nonlinear autonamous flows.

1.2. Nonlinear Systems

Systems whose behaviour can not be represented as linear sum of the behaviours of their parts are called nonlinear systems. Their behaviour is not subject to the principles of superposition theory. That is why nonlinear systems show considerably richer and more complex behaviours than linear systems. Their behaviours can be categorized as follows:

1- Equilibrium Points: An equilibrium point is a point where the system can stay forever without moving. Nonlinear systems generally have more than one equilibrium point. They can be classified as:

a- Stable Equilibrium Points: An equilibrium is defined to be stable if all sufficiently small disturbances away from it damp out in time.

b- Unstable Equilibrium Points: An equilibrium is defined to be unstable if all sufficiently small disturbances away from it grow in time.

c- Saddle Points: An equilibrium is defined to be saddle if it owns both the stable and unstable manifold.

2- Stable Limit Cycle: A stable limit cycle is a closed trajectory in phase space into which at least one another trajectory spirals as time approaches infinity.

3- Marginally Closed Trajectories: Trajectories swirls around a linear and nonlinear center and form a periodic motion.

4- Chaos: Chaotic behaviour which is characterized by the sensitivity to initial conditions can be observed mostly in strong nonlinear systems. As a result of this sensitivity chaotic systems exhibit random-like behaviour even though they are 'deterministic' in the sense that their future states are causally determined by their present states. Chaos can be experienced only in three or higher dimensional systems.

In this thesis, we will identify the invariant sets, which are formed during the behaviours mentioned above, from a sufficiently large set of system data.

Definition: Invariant Sets

In a time-invariant nonlinear system $\dot{x} = f(x)$, a set $G \subseteq R^n$ is invariant if every trajectory $x(t)$ satisfies:

$$x(t) \in G \Rightarrow x(r) \in G \quad \forall r \geq t \quad (1.2)$$

Definition: Attractors

An attractor can be defined as a set to which all neighboring trajectories converge. The following condition must be satisfied to name a set "A" an attractor:

- 1- A must be closed.
- 2- A is an invariant set. Any trajectory $x(t)$ that enters A or starts in A , stays in A for all time.
- 3- A attracts an open set of initial conditions. There is an open set U containing A such that if $x(0) \in U$, then the distance from $x(t)$ to A tends to zero as $t \rightarrow \infty$. This means that A attracts all trajectories that start sufficiently close to it. The largest such U is called the basin of attraction of A . In other words, basin of attraction is the set of points in the space of system variables such that initial conditions chosen in this set dynamically evolve to a particular attractor.
- 4- A is minimal. There is no proper subset of A that satisfies conditions 1, 2 and 3.

Invariant sets sometimes behave like boundaries in phase space and they restrict trajectories inside it to a subset of phase space.

The state space regions corresponding to the same long term behaviour will be referred to as basin. The long term behaviours of interest in this thesis will consist of attractors, exit basins and marginal basins. For attractors, these basins will be the basin of the stable equilibrium point or stable limit cycle. Note that all these basins will be searched in a region of interest (ROI) of state space which is chosen prior to analysis.

During this thesis we will focus on basin of attraction of stable equilibrium points, limit cycles, centers, asymptotes and exit boundary segments. We will use mainly kernel estimators, parametric regressions and our novel algorithms to detect and identify these invariant sets. The detection and identification of the behaviour types of different regions in phase space can be used in future for control purposes of nonlinear dynamical systems.

1.3. Regression Types

Given a set of random variables X_1, X_2, \dots, X_n with a continuous joint probability density $f(X_1, X_2, \dots, X_n)$ and without knowledge of real f , we are looking for a specific structure in our data. This unknown joint probability density can be estimated from a set of observations using parametric or nonparametric regressions.

Assume that X is the predictor of Y , which is called as the response variable. In this case,

$$Y = m(X) + e \quad (1.3)$$

where,

$m(X)$: the best mean squared predictor of Y and is called the regression of Y on X .

e : the observational error which is a symmetric random variable having zero mean.

$$E(e) = 0.$$

In parametric regression, parametric family of functions are used to estimate the original function. It is assumed that the regression function, $m(X)$, is known except for the values of the parameters. Typical example functions used in parametric regression are:

$$Y_i = \alpha_0 + \alpha_1 X_i + \alpha_2 X_i^2 + e_i \quad (1.4)$$

$$Y_i = \alpha_1 \sin(\alpha_2 X_i) + e_i \quad (1.5)$$

$$Y_i = \alpha_1 / (\alpha_2 + X_i) + e_i \quad (1.6)$$

where,

X_i : the i 'th sample of the data

Y_i : the corresponding response, the value that is estimated.

The drawback of this method is the restriction of regression function belonging to a parametric family. In some situations this choice may be too rigid. For example, the model requires that $m(X)$ to be sinusoidal which can be very restrictive for a proper estimation of the original function. There is a high possibility to reach incorrect results in the estimation process. This rigidity can be overcome by the second method where the restriction of $m(X)$ belonging to a specific family of functions is removed.

In nonparametric regression, the model structure is not specified a priori. Instead of a specific parametric function, it is determined from data. In this regression type, it is not

meant to mention that they completely lack parameters. They rather are flexible at the nature and number of parameters. In some cases, parametric models may also be estimated by the nonparametric regression.

2. MATHEMATICAL BACKGROUND

2.1. Analysis of Non-Linear Dynamical Systems

Definition: Nonlinear Systems

Systems whose behaviour can not be represented as linear sum of the behaviours of their parts are called nonlinear systems. Their behaviour is not subject to the principles of superposition theory.

A general model used for nonlinear systems is:

$$\dot{\underline{x}}(t) = f(t, \underline{x}(t), \underline{u}(t)) \quad \forall t \geq 0, \underline{x}(t) \in R^n, \underline{u}(t) \in R^m \quad (2.1)$$

where,

t: time

$\underline{x}(t)$: n-dimensional vector which denotes the value of the function $\dot{\underline{x}}(t)$ at time t, that is to say it is the state vector of the system.

$\underline{u}(t)$: m-dimensional input vector of the system. Systems which have an input vector are said to be *forced*.

Definition: Autonomous Systems

Any nonlinear system is said to be autonomous if the function f does not depend explicitly on time. Time invariant systems can be represented as $\dot{\underline{x}}(t) = f(\underline{x}(t))$.

Note that this is an unforced system since it does not have any external input vector. In this thesis, we will concentrate on the analysis and estimation of two dimensional unforced, autonomous nonlinear systems.

2.1.1. Two Dimensional Systems

Two dimensional autonomous systems have a significant importance in nonlinear analysis. The solution trajectories can be drawn by using curves in the plane and this allows us to visualize the system behaviour easier.

The general representation of second order autonomous systems are:

$$\begin{aligned}\dot{x} &= f_1(x, y) \\ \dot{y} &= f_2(x, y)\end{aligned}\tag{2.2}$$

$f_1(x, y)$ and $f_2(x, y)$ will be thought as vector fields on the phase plane. On each point x in the plane, a vector $f(x, y)$ will be assigned, a directed line segment from x to $x + f(x, y)$. After repeating this process at every single state, we obtain a vector field diagram of our nonlinear system. The vector field is tangent to the trajectory through that point. If this construction is made with a family of different initial conditions, the phase portrait of the system is drawn.

We will try to determine the qualitative behaviour of the system from the phase portrait but first we need to define analytically the fundamental features of a phase portrait of linear dynamical systems to have a better understanding of nonlinear systems.

2.1.2. Phase Plane Analysis in Linear Systems

The general form of a linear second-order system:

$$\begin{aligned}\dot{x} &= a_1x + a_2y \\ \dot{y} &= a_3x + a_4y\end{aligned}\tag{2.3}$$

From the equation 2.3, \dot{y} can be expressed as:

$$a_2\dot{y} = a_2a_3x + a_4\dot{x} - a_1a_4x\tag{2.4}$$

Differentiation of the equation 2.3 gives

$$\ddot{x} = a_1 \dot{x} + a_2 \dot{y} \quad (2.5)$$

and a substitution of equation 2.4 into equation 2.5 gives

$$\ddot{x} = (a_1 + a_4) \dot{x} + (a_2 a_3 - a_1 a_4) x \quad (2.6)$$

Hence, a general form of second order linear systems is reached:

$$\ddot{x} + a\dot{x} + bx = 0 \quad (2.7)$$

The analytical solution of this linear system is:

$$x(t) = e^{\lambda_1 t} v_1 + e^{\lambda_2 t} v_2 \quad \text{if } \lambda_1 \neq \lambda_2 \quad (2.8)$$

$$x(t) = e^{\lambda_1 t} v_1 + t e^{\lambda_2 t} v_2 \quad \text{if } \lambda_1 = \lambda_2 \quad (2.9)$$

where,

v_1 and v_2 are the eigenvectors

λ_1 and λ_2 are the eigenvalues of the characteristic equation:

$$s^2 + as + b = (s - \lambda_1)(s - \lambda_2) = 0 \quad (2.10)$$

λ_1 and λ_2 can be solved for:

$$\lambda_1 = \frac{-a + \sqrt{a^2 - 4b}}{2} \quad \text{and} \quad \lambda_2 = \frac{-a - \sqrt{a^2 - 4b}}{2} \quad (2.11)$$

As long as λ_1 and λ_2 are distinct, the corresponding eigenvectors are linearly independent too and can span the entire phase plane.

Definition: Equilibrium Points

A vector $\underline{x}_o \in R^n$ is said to be an equilibrium if

$$f(t, \underline{x}_o) = 0 \quad \forall t \geq 0 \quad (2.12)$$

If a system starts in an equilibrium, it remains in that state for ever. We can find the equilibrium of a system by finding where the flow zero is. So, solving $\dot{x} = 0$ and $\dot{y} = 0$ for linear systems always give the solution $x = 0$ and $y = 0$, that is to say the origin. However depending on the values of a and b , the eigenvalues take different signs or own an imaginary part which results in different behaviour characteristics around the origin. The fundamental behaviour types are summarized below:

Stable / Unstable Node : If both eigenvalues are negative and real, then both $x(t)$ and $\dot{x}(t)$ converge to zero exponentially, that is to say the equilibrium point is stable. If both eigenvalues are positive and real, then $x(t)$ and $\dot{x}(t)$ diverge exponentially and states of the system blow up. Hence, the equilibrium point is said to be unstable.

Saddle Point : If one eigenvalue is positive and other one is negative, then a phenomena called “saddle point” is observed. Due to the stable node two trajectories form the stable manifold of the saddle point. All the other trajectories diverge from the saddle point.

Stable / Unstable Focus : If the eigenvalues have an imaginary part and if their real part are negative, then trajectories form a stable spiral around the equilibrium point. If the real parts of the eigenvalues are positive, then the trajectories near the equilibrium point diverge from it to infinity by forming an outwards spiral.

Center Point : If the trajectories around the equilibrium point swirl and circulate, then it is said that the trajectories are closed orbits and the equilibrium point is a center. The

behaviour of the state can be expressed as a periodic motion or as an oscillation between two points.

2.1.3. Phase Plane Analysis in Non-Linear Systems

The phase portrait analysis of nonlinear systems can be interpreted by linear system phase plane analysis because the local behaviour of a nonlinear system can be approximated most of the time by the behaviour of linear system. Nonlinear systems can exhibit more complicated phenomena than linear systems like limit cycles, multiple equilibrium points and even chaos.

Consider the system

$$\begin{aligned}\dot{x} &= f_1(x, y) \\ \dot{y} &= f_2(x, y)\end{aligned}\tag{2.13}$$

Suppose that (\hat{x}, \hat{y}) is the equilibrium point so that

$$\dot{x} = f_1(\hat{x}, \hat{y}) = 0 \quad \text{and} \quad \dot{y} = f_2(\hat{x}, \hat{y}) = 0\tag{2.14}$$

Let the small disturbances around the equilibrium point to be:

$$u = x - \hat{x} \quad \text{and} \quad v = y - \hat{y}\tag{2.15}$$

Differentiation of u and v , substitution to equation 20 and at last expansion by Taylor series give us:

$$\begin{aligned}\dot{u} &= \dot{x} \\ \dot{u} &= f_1(\hat{x} + u, \hat{y} + v) \\ \dot{u} &= f_1(\hat{x}, \hat{y}) + u \frac{\partial f_1}{\partial x} + v \frac{\partial f_1}{\partial y} + O(u^2, v^2, uv) \\ \dot{u} &= u \frac{\partial f_1}{\partial x} + v \frac{\partial f_1}{\partial y} + O(u^2, v^2, uv)\end{aligned}\tag{2.16}$$

$$\begin{aligned}
\dot{v} &= \dot{x} \\
\dot{v} &= f_2(\hat{x} + u, \hat{y} + v) \\
\dot{v} &= f_2(\hat{x}, \hat{y}) + u \frac{\partial f_2}{\partial x} + v \frac{\partial f_2}{\partial y} + O(u^2, v^2, uv) \\
\dot{v} &= u \frac{\partial f_2}{\partial x} + v \frac{\partial f_2}{\partial y} + O(u^2, v^2, uv)
\end{aligned} \tag{2.17}$$

where,

$\frac{\partial f}{\partial x}$ and $\frac{\partial f}{\partial y}$ are evaluated at the equilibrium points (\hat{x}, \hat{y})

$O(u^2, v^2, uv)$ is the quadratic terms in u and v after Taylor series expansion

$f_1(\hat{x}, \hat{y})$ and $f_2(\hat{x}, \hat{y})$ are equal to zero since (\hat{x}, \hat{y}) are numbers.

Assuming that quadratic terms do not have a significant effect in a small area around the equilibrium point, they can be neglected and the rest can be expressed in a matrix form to reach the familiar form of linear systems:

$$\begin{bmatrix} \dot{u} \\ \dot{v} \end{bmatrix} = \begin{bmatrix} \frac{\partial f_1}{\partial x} & \frac{\partial f_1}{\partial y} \\ \frac{\partial f_2}{\partial x} & \frac{\partial f_2}{\partial y} \end{bmatrix} \begin{bmatrix} u \\ v \end{bmatrix} \tag{2.18}$$

The dynamics of this system can be analyzed by the linear methods explained in the previous section.

Example: Consider the second order nonlinear dynamical system as described below:

$$\begin{aligned}
\dot{x} &= y \\
\dot{y} &= -(0.6y + 3x + x^2)
\end{aligned}$$

To find the equilibrium of the system where there is no flow $f_1(x, y) = 0$ and $f_2(x, y) = 0$ should be solved. The necessary calculations show that the above system has two equilibrium points, one at $x = 0$, $y = 0$ and the other at $x = -3$, $y = 0$.

$$\begin{bmatrix} \dot{u} \\ \dot{v} \end{bmatrix} = \begin{bmatrix} 0 & 1 \\ -3-2x & -0.6 \end{bmatrix} \begin{bmatrix} u \\ v \end{bmatrix} \Rightarrow s(s+0.6) + 3 + 2x = 0$$

$$(0,0) \Rightarrow s(s+0.6) + 3 = s^2 + 0.6s + 3 \Rightarrow \lambda_1 \approx -0.3 - 1.7i \text{ and } \lambda_2 \approx -0.3 + 1.7i$$

$$(-3,0) \Rightarrow s(s+0.6) - 3 = s^2 + 0.6s - 3 \Rightarrow \lambda_1 \approx 1.46 \text{ and } \lambda_2 \approx -2.06$$

Hence, we have a stable focus at $(0,0)$ and a saddle point at $(-3,0)$.

Although in most cases, higher order nonlinear terms can be neglected without causing qualitative approximation errors, in some cases avoiding these terms may give us incorrect pictures. However the marginal cases like centers, or non-isolated equilibrium points (equilibrium lines) can easily be disturbed by small perturbations, that is to say the quadratic terms in the Taylor series play a critical role in the nature of the system. So, if these marginal cases are encountered after linearization, the result will not be trustable and other analytical tools should be used to identify the real characteristic nature of the dynamical system.

Since we investigate the dynamical systems totally from a geometric point of view, (rather than being analytical), we will never be in the danger zone mentioned above.

2.1.4. Limit Cycle

In nonlinear dynamics, the system nature is not limited to have only equilibrium points and a continuum of periodic orbits. More complicated behaviours like limit cycles can be observed too.

If a trajectory in a nonlinear system is closed and isolated, that is to say have a periodic nature of the motion, and all nearby trajectories converges to it or diverges from it, then it is called a limit cycle.

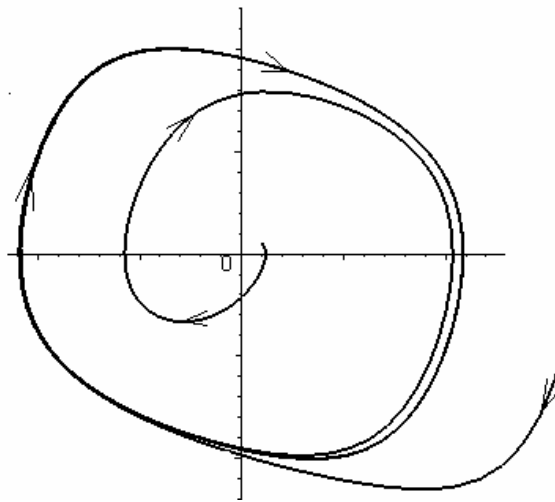


Figure 2.1. Limit Cycle

Limit cycles can be classified according to their stability.

1- *Stable Limit Cycle*: All trajectories in the vicinity of the limit cycle converge to the limit cycle as $t \rightarrow \infty$.

2- *Unstable Limit Cycle*: All trajectories in the vicinity of the limit cycle diverge from the limit cycle as $t \rightarrow \infty$.

3- *Semi-Stable Limit Cycle*: In the vicinity of either inside or outside of the limit cycle, some trajectories converge to the limit cycle and the others diverge from the limit cycle as $t \rightarrow \infty$.

2.2. Regression Models and Kernel Estimators

2.2.1. Histograms and Univariate Kernel Estimator

In many parts of the thesis regression methods will be used to provide analytical description of attractors, asymptotes and basin of attractors. Therefore they are important tools and deserve to be introduced in detail.

Definition : Frequency distribution

The tabulation of raw data obtained by dividing it into classes of some size and computing the number of data elements (or their fraction out of the total) falling within each pair of class boundaries is called frequency distribution.

If we examine the frequency of which states fall into a given region of the state space at a specific time, we observe the state probability density.

Definition : Density function

A function $f_0(x)$ is the density function for the initial states $x_1^o, x_2^o, \dots, x_N^o$ if for every (not too small) interval $\Delta_0 \subset [0,1]$

$$\int_{\Delta_0} f_o(u) du \cong \frac{1}{N} \sum_{j=1}^N \Delta_0(x_j^o) \quad (2.19)$$

where

$$\Delta(x) = 1 \quad \text{if } x \in \Delta$$

$$\Delta(x) = 0 \quad \text{if } x \notin \Delta$$

The oldest, simplest and most frequently encountered nonparametric regression estimator for probability density function is the histogram. To construct a histogram, the interval covered by the data is divided into equal bins, i.e. equally sized intervals. The width of the bin and starting position of the histogram have great effects on the overall shape of the histogram. A generalized formula can be stated as:

$$f(x,b) = \frac{m}{nb} \quad (2.20)$$

where,

b : the width of the bins

n : number of random variables, samples

m : number of observations in bin containing x

The effects of these factors are explained with an example.

Consider 40 random numbers that are generated in the range $[0,1]$

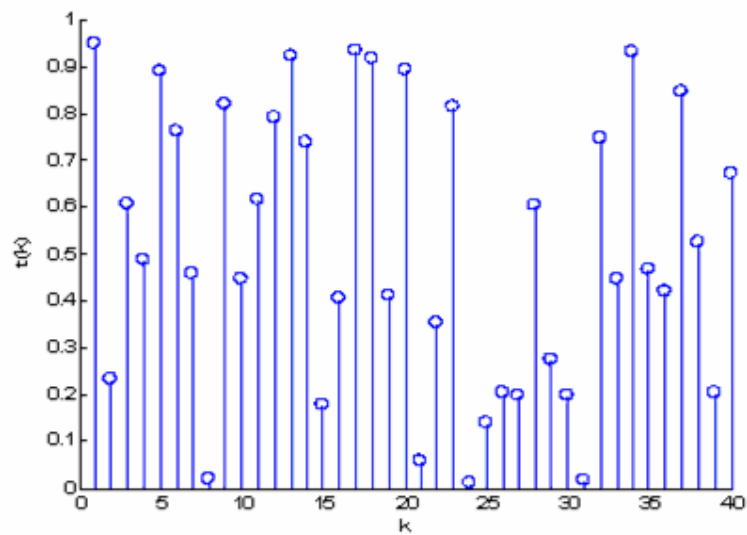


Figure 2.2. 40 Random Numbers between 0-1

Two histograms are shown for this data (Figure 2.3.). Although they only differ at their starting point by 0.05 they look quite different.

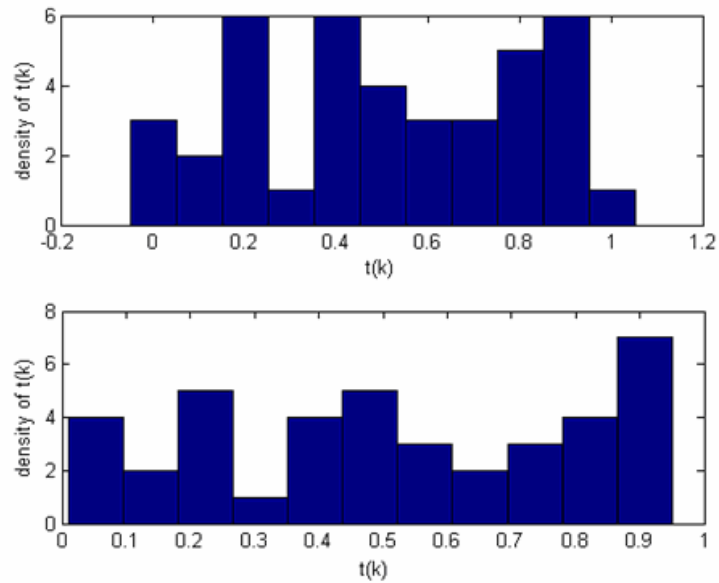


Figure 2.3. Histograms with Different Starting Points

In figure 2.4, two histograms for the same data set are drawn. With the difference of the bandwidth of the second histogram some details, like the bimodality structure around 0.85 are missed in the first histogram.

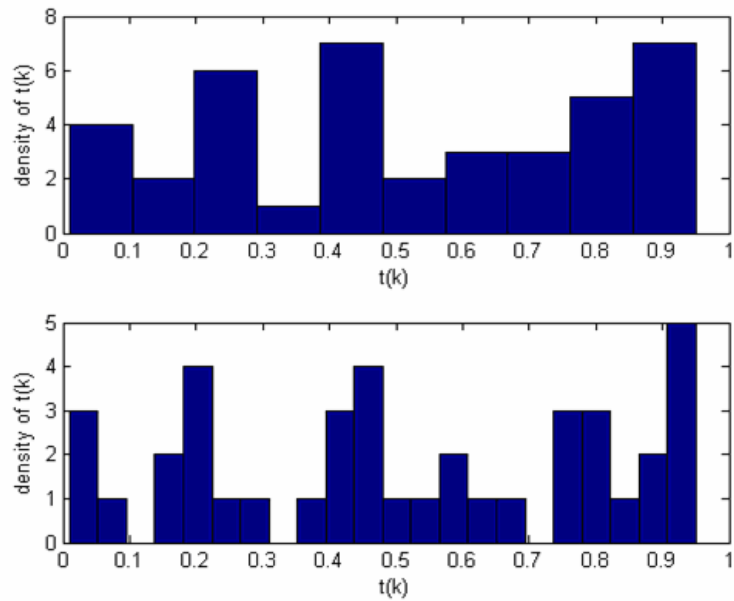


Figure 2.4. Histograms with Different Bandwidths

As conclusion, histograms are not smooth and depend highly on the start points and widths of the bins. The dependence on the start points and the smoothness problems can be alleviated by another nonparametric estimator: Kernel estimators.

If we use a smooth kernel function instead of a box shaped function for our building block, then we will have a smooth density estimate. To remove the dependence on the start position of the bins, we center each kernel function at each data point instead of fixing their start points. This way two important problems associated with histograms are eliminated.

The generalized formula for kernel density estimators is:

$$f(x, h) = \frac{1}{nh} \sum K\left(\frac{x - X_i}{h}\right) \quad (2.21)$$

where,

K : the kernel function

X_i : random sample taken from a continuous univariate density function, i.e. observations

h : bandwidth of the kernel function

For one dimensional case the performance of the kernel density estimator is measured by the appropriate error criteria over the whole line, MISE or AMISE.

Definition : Mean Squared Error , Mean Integrated Square Error and Asymptotically MISE.

$$MSE(m) = E(m - p)^2 \quad (2.22)$$

where,

p: the original, estimated density.

m: the estimator.

To interpret data in the entire line instead of a single point we use MISE :

$$MISE(f(x, h)) = E \int (f(x, h) - g(x))^2 dx \quad (2.23)$$

where,

$g(x)$: the original estimated density function.

$f(x, h)$: the estimator function.

h : the bandwidth of the estimator function

Due to the high complexity of the open form of MISE, the AMISE (is introduced:

$$AMISE(f(x, h)) = \frac{1}{nh} R(K) + \frac{1}{4} h^4 \mu_2 K^2 R(\ddot{f}) \quad (2.24)$$

where,

n : number of samples

K : Kernel function

$$R(m) = \int m(x)^2 dx$$

$$\mu_2(K) = \int z^2 K(z) dz$$

AMISE is a useful sample approximation to the MISE and it is a much simpler expression compared the open expression of MISE.

When AMISE is used to to measure the efficiency of several kernel functions, we can see that the shape of the kernel function does not have much effect on the estimation. However, the bandwidth can greatly change the overall appearance of the estimated density.

To take a deeper look into the concepts mentioned above, the well known Logistic Map will be represented as an example. The logistic map is a well known example of chaotic behavior that arises from a very simple nonlinear equation. The map is given by:

$$x_{n+1} = rx_n(1 - x_n) \quad (2.25)$$

The trajectory for the first 100 iterations of the logistic map where r is taken as 4 and the initial point is 0.22, is drawn below.

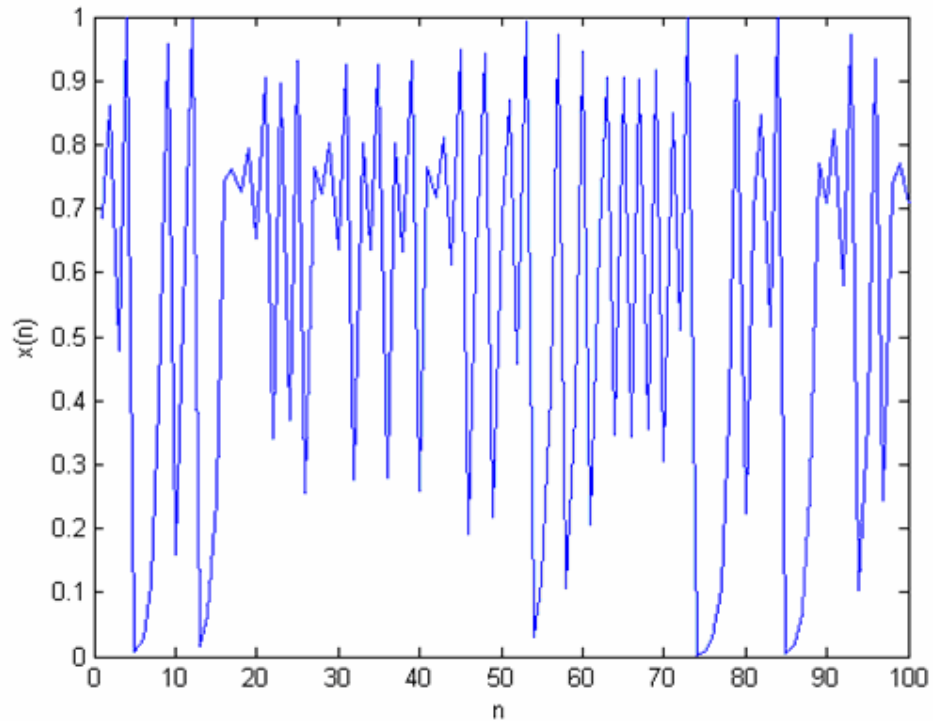


Figure 2.5. Trajectory for Logistic Map

If the state density is estimated by Parzen's estimator given by

$$f(x, h) = \frac{1}{nh} \sum g\left(\frac{x - X_i}{h}\right) \quad (2.26)$$

where the Gaussian Kernel function defined by

$$g(x) = (2\pi)^{-0.5} e^{-0.5x^2} \quad (2.27)$$

is used. Different results for different bandwidths can be obtained.

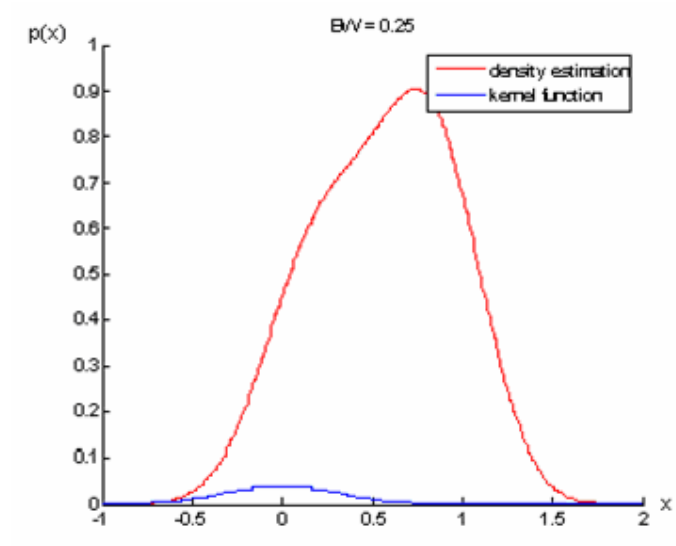


Figure 2.6. Oversmoothed Estimate

The shape is too smooth and the characteristic details associated with the states disappeared. Such an estimate is called oversmoothed.

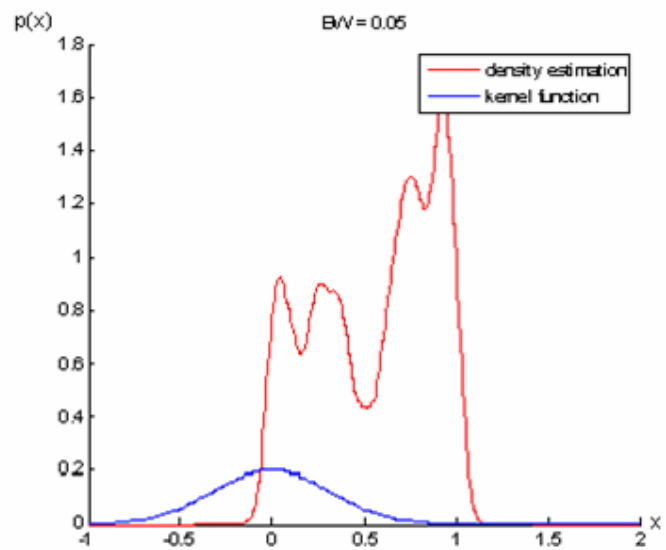


Figure 2.7. Undersmoothed Estimate

Letting $h = 0.05$, the estimate pays too much attention to specific data and it is not smoothed enough. The estimate is then called to be undersmoothed.

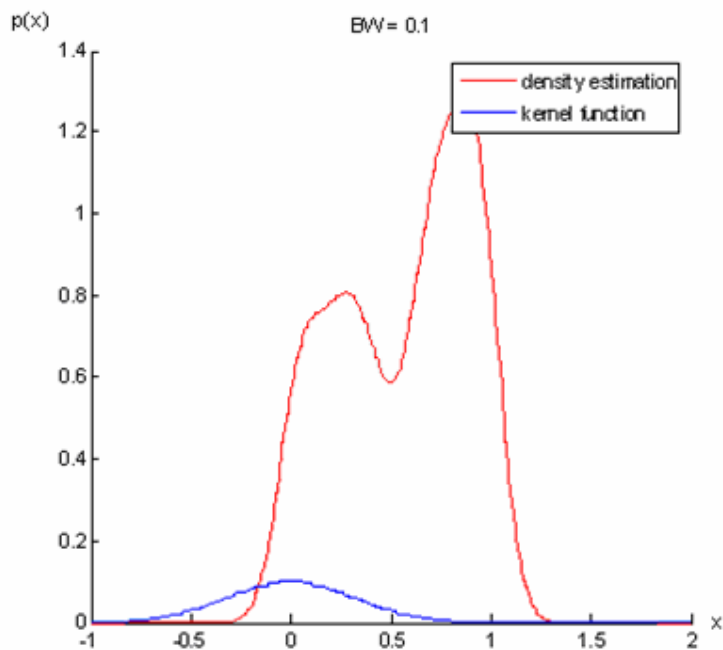


Figure 2.8. Optimum Estimate

The case where the bandwidth is very close to the optimum bandwidth which is calculated by minimizing AMISE ($BW=0.00997$), is shown in Figure 2.8. Around this bandwidth, the kernel estimate is not too noisy and the essential structure can be recovered.

2.2.2. Multivariate Kernel Estimation

The main reason that relatively less research has been done about the kernel estimation for multivariate data is that they are far more complicated than the univariate case both in computational and mathematical aspects. One of important difference is the selection of bandwidth matrix that may induce an orientation of the kernel function. The determination of the bandwidth matrix and the variation of the parameters have no univariate analogue.

The kernel density estimation for univariate data has received significant attention in the literature, however the multivariate density estimation has been given less importance. This is partly due to the visualization difficulties of high dimensional data. Although some visualization techniques has been proposed, interpretation of the resulting plots are not easy and needs experience.

A simple extension of the univariate kernel estimation is not enough in most situations due to the more complicated bandwidth settings. Furthermore, the sparseness of data in higher-dimensional space make kernel smoothing more difficult if the sample size is not very large. This results in the lack of proper estimation for the systems with practical sample sizes that have more than five dimensions. This difficulty is called the curse of dimensionality. That is why especially in diagrams and plots, bivariate kernel density estimation will be used as an example. The bivariate kernel estimator is a bridge between the univariate and high-dimensional kernel density estimation. Furthermore the bivariate kernel extensions can be visualized by simple contours. This forms the first step for understanding different aspects of the multivariate kernel smoothing. To investigate the multivariate kernel estimation, first its definition will be given.

Definition: Multivariate kernel estimator

Let $X = (X_1, X_2, \dots, X_d)^T$ denote a d-dimensional random vector with density $f(x)$ defined on R^d . The general form of the multivariate kernel estimator is:

$$f(x, H) = n^{-1} \sum_{i=1}^n K_H(x - X_i) \quad (2.28)$$

where,

$$K_H(x) = |H|^{-0.5} K(H^{-0.5}x) \quad (2.29)$$

and H is a symmetric positive definite $d \times d$ matrix known as the bandwidth matrix, $K(\cdot)$ is a multivariate kernel function satisfying :

$$\int K(x) dx = 1 \quad (2.30)$$

The roots of the multivariate kernel density estimators were based on the second half of 1960's. The bandwidth selection forms the basis of the multivariate kernel estimation problem. The parameters of the bandwidth matrix control the orientation of the kernel function. There are 3 main classes and 3 hybrid classes for bivariate data case:

1- class of all symmetric, positive definite matrices :

$$H = \begin{bmatrix} h_1^2 & h_{12} \\ h_{12} & h_2^2 \end{bmatrix} \quad (2.31)$$

2- class of all diagonal, positive definite matrices:

$$H = \begin{bmatrix} h_1^2 & 0 \\ 0 & h_2^2 \end{bmatrix} \quad (2.32)$$

3- class of all positive constants multiplied by the identity matrix:

$$H = \begin{bmatrix} h^2 & 0 \\ 0 & h^2 \end{bmatrix} \quad (2.33)$$

4- class of all positive constants multiplied by the sample variance S:

$$H = \begin{bmatrix} h^2 S_1^2 & h^2 S_{12} \\ h^2 S_{12} & h^2 S_2^2 \end{bmatrix} \quad (2.34)$$

5- class of all positive constants multiplied by the sample variance:

$$H = \begin{bmatrix} h^2 S_1^2 & 0 \\ 0 & h^2 S_2^2 \end{bmatrix} \quad (2.35)$$

6- class of matrices formed by correlation coefficient ρ :

$$H = \begin{bmatrix} h_1^2 & \rho_{12} h_1 h_2 \\ \rho_{12} h_1 h_2 & h_2^2 \end{bmatrix} \quad (2.36)$$

The second class of bandwidth matrices are the most commonly used in literature so far. Each bandwidth type can be inappropriate for specific cases. For example, the target density shown in Figure 2.9. can not be estimated properly by the kernel function shown in Figure 2.9.

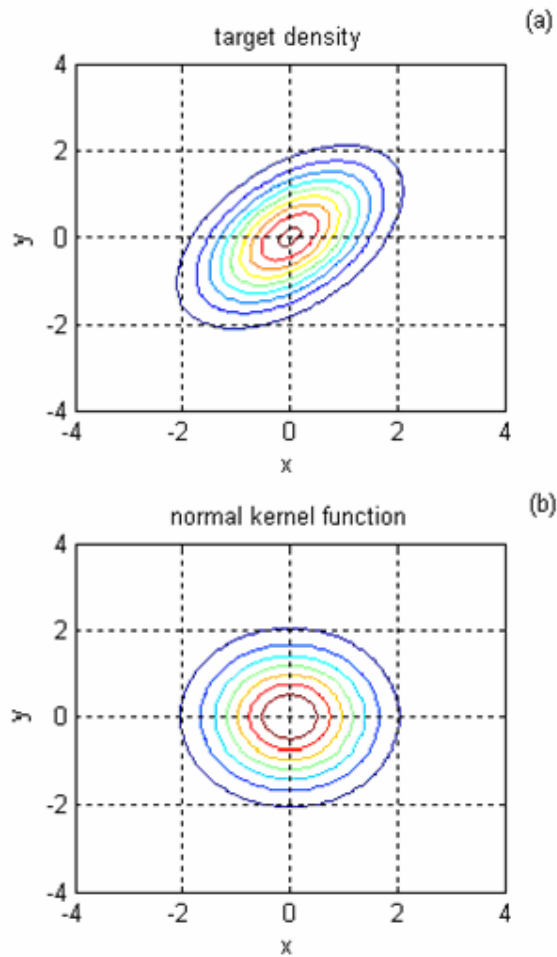


Figure 2.9. Density Example and 2D Kernel Function

The probability mass of the target density function is oriented along $y=x$ line, however the kernel used for the estimation is perfectly symmetric around the $x-y$ axis. Since the distribution of the mass probabilities of both functions are not matched, it is

impossible to estimate the original function in Figure 2.9. with the kernel in Figure 2.9. properly.

In this thesis, we will mostly select the bandwidth of Kernel functions in the form of equation 38 which is a diagonal positive constant matrix. In the additional work and different approaches section of the thesis, we will select bandwidth according to the location of the estimated data on the phase plane:

$$H = \begin{bmatrix} h^2(x, y) & 0 \\ 0 & h^2(x, y) \end{bmatrix} \quad (2.37)$$

2.2.3. Parametric Regression

The nonparametric regression is used to identify the attractors on the phase plane. However for the representation of basins of attraction analytically, parametric regression models are used.

To estimate the function of the basins of attraction, the following models are proposed:

$$\text{Second order polynomial: } y = ax^2 + bx + c \quad (2.38)$$

$$\text{Third order polynomial: } y = ax^3 + bx^2 + cx + d \quad (2.39)$$

$$\text{General ellipse: } ax^2 + bxy + cy^2 + dx + ey + f = 0 \quad (2.40)$$

$$\text{Nonlinear hyper surface: } ax^2y^2 + bxy^2 + cy^2 + dx^2y + ex^2 + fxy + gx + hy + i = 0 \quad (2.41)$$

The user is free to choose any of these models to fit the data in any of the basins of attraction.

The unknown coefficients in equation 43 and 44 are computed by minimizing the sum of the squares of the deviations of the data from the proposed polynomials. For the nonlinear models, Gauss-Newton method is used for least square-data fitting.

If the model does not fit good enough, the regression should be repeated with another model.

Example: Suppose we have the data points distributed as shown in figure 2.10.

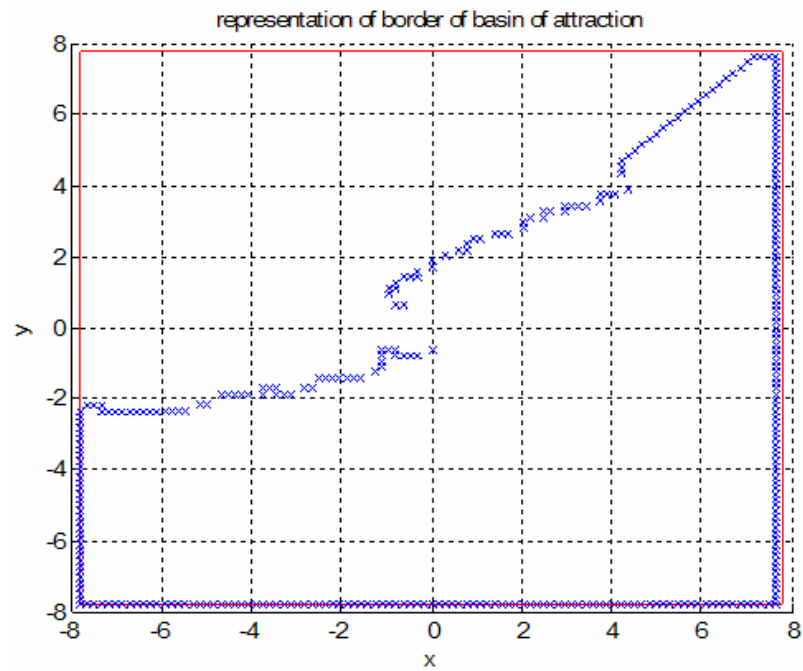


Figure 2.10. Sample of Data Points

Parametric estimation using the model in equation 45 gives a result which roughly covers the region of interest

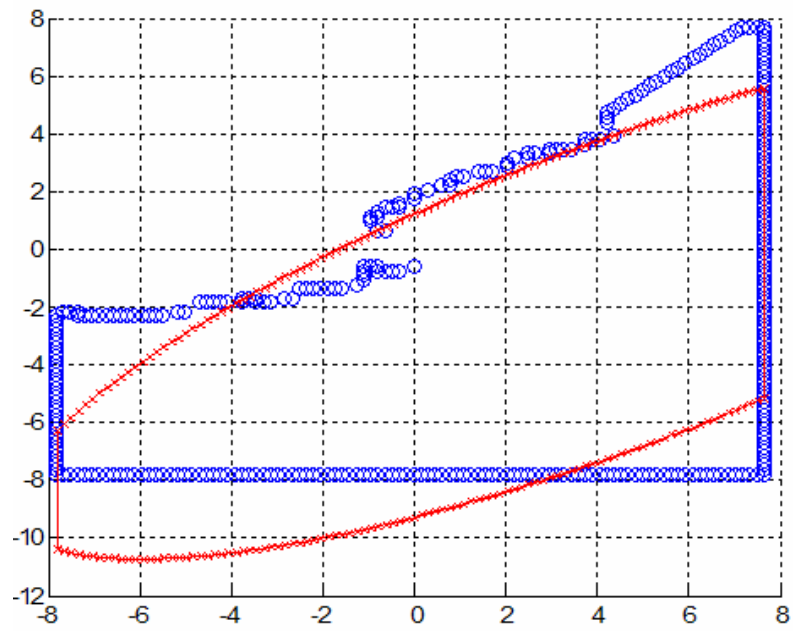


Figure 2.11. Estimation of the Boundary with 3. Model

However 4. model gives a superior estimate than the third model:

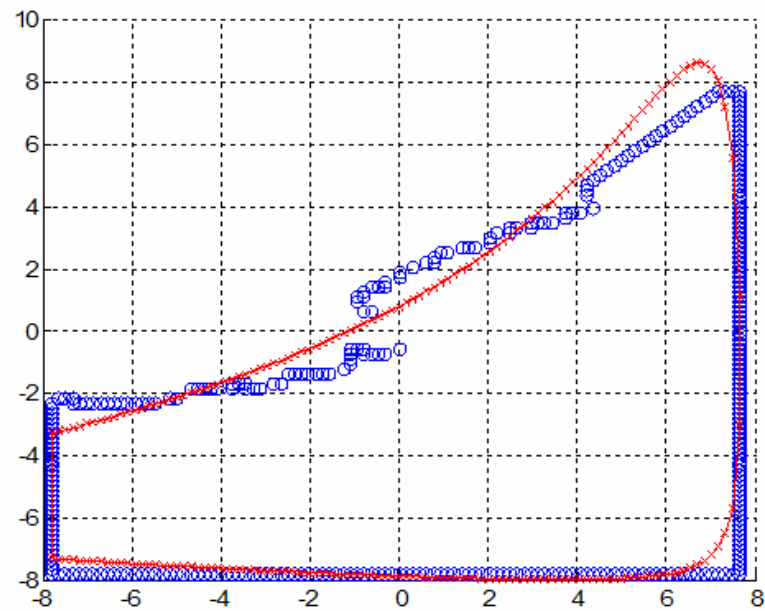


Figure 2.12. Estimation of the Boundary with 4. Model

3. METHODOLOGY

During our thesis, it is assumed that

- 1- Equations governing the dynamical system are not known.
- 2- The system dimension is not known.
- 3- There is a sufficient number of trajectory observations starting from different initial conditions.

Moreover this thesis is focused on systems which

- do not exhibit chaotic behaviour.
- have only stable/unstable nodes, stable/unstable focuses, saddle points, periodic orbits or limit cycles.
- do not have more than one limit cycle or continuum of periodic orbits.

Under these assumptions, in order to identify and extract the characteristic regions of basins of the nonlinear system the following methods are used:

- Kernel Regression
- Parametric Regression
- Poincare Maps
- Basic image processing technics
- “Flame Expansion” algorithm to identify the basin boundaries

3.1. Identification of Stable Equilibrium Points

Trajectories which converge to a stable equilibrium point must have a higher state density near the equilibrium point.

So, it is checked if the last n -points of each trajectory are in a small circle around the last point of each trajectory. The radius is determined by the user. Note that an optimum selection of radius of this circle is assumed to have a correlation with the the average distance of each data point in each trajectory.

After finding the equilibrium point candidates, Kernel Regression is used to estimate the exact location of the equilibrium points.

Example:

Consider the system below.

$$\begin{aligned}\dot{x} &= y \\ \dot{y} &= -(8 + x^2)y + 3x - x^3\end{aligned}$$

The phase portrait of this system with initial conditions

$$\begin{aligned}x_0 &= [-2.5 \quad -2.2 \quad -1.9 \quad \dots \quad 2.3] \\ y_0 &= [-2.5 \quad -2.2 \quad -1.9 \quad \dots \quad 2.3]\end{aligned}$$

is shown below.

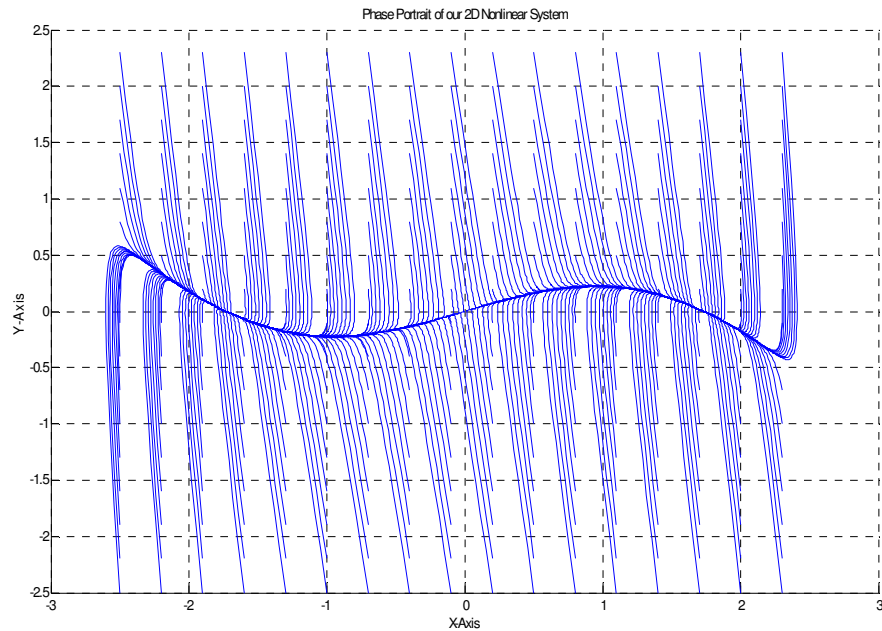


Figure 3.1. Phase Portrait of the 2D-Example

After checking each trajectory if it satisfies the criteria mentioned above, the last point of the trajectories that shows a sign of an equilibrium point is marked.

In figure 3.2, there are two main groups of equilibrium point candidates.

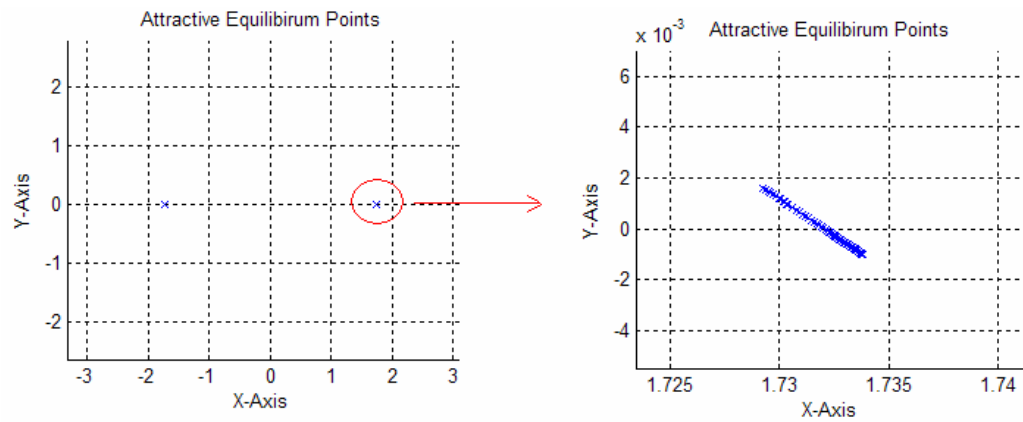


Figure 3.2. Equilibrium Point Candidates

Now, a kernel function is placed on each candidate. After each kernel function is added, the local peaks are determined.

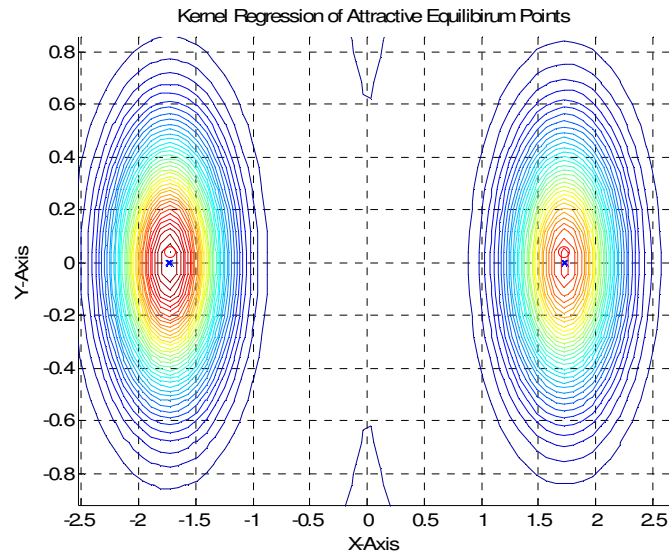


Figure 3.3. Kernel Regression of Equilibrium Point Candidates

The local peaks of the Kernel functions are found to be on

$$x_1^*, y_1^* = [-1.7286 \quad 0.0402] \text{ and } x_2^*, y_2^* = [1.7286 \quad 0.0402]$$

This result corresponds with the analytical solution of the attractive equilibrium points.

$$\dot{x} = 0 \rightarrow y = 0$$

$$\dot{y} = 0 \rightarrow 3x - x^3 = 0 \rightarrow x_1 = 0; x_2 = \sqrt{3} \approx 1.7321; x_3 = -\sqrt{3} \approx -1.7321$$

The linearized analysis of the Jacobian Matrix give us that (0,0) is a saddle point and other two equilibrium points are stable nodes.

3.2. Identification of Periodic Orbits and Limit Cycles

To identify periodic orbit and limit cycle phenomena, Poincare maps are used. One horizontal and one vertical Poincare line are placed at the bottom left of the phase portrait. Then it is checked if there are at least 3 three points in each Poincare line and if the difference between the first and third point is small enough. Theoretically, this difference should be zero since a periodic orbit intersects a Poincare Line exactly at the same point and forms a fixed equilibrium point in the Poincare map which corresponds to a periodic orbit in the nonlinear system. However due to the sampled data structure, interpolations to find the intersection point of the Poincare line and the trajectories have been made. One of the drawbacks of this interpolation is that the intersection points may be separated from each other within a small distance. It is assumed that if this distance is small enough, then an equilibrium point in the Poincare line is found and hence the nonlinear system exhibits periodic behaviour.

If we can not catch at least 3 points on none of the Poincare lines, then both lines are slided and the iterations are repeated until all the phase plane is covered.

Below, a horizontal Poincare line near a nonlinear closed orbist is shown.

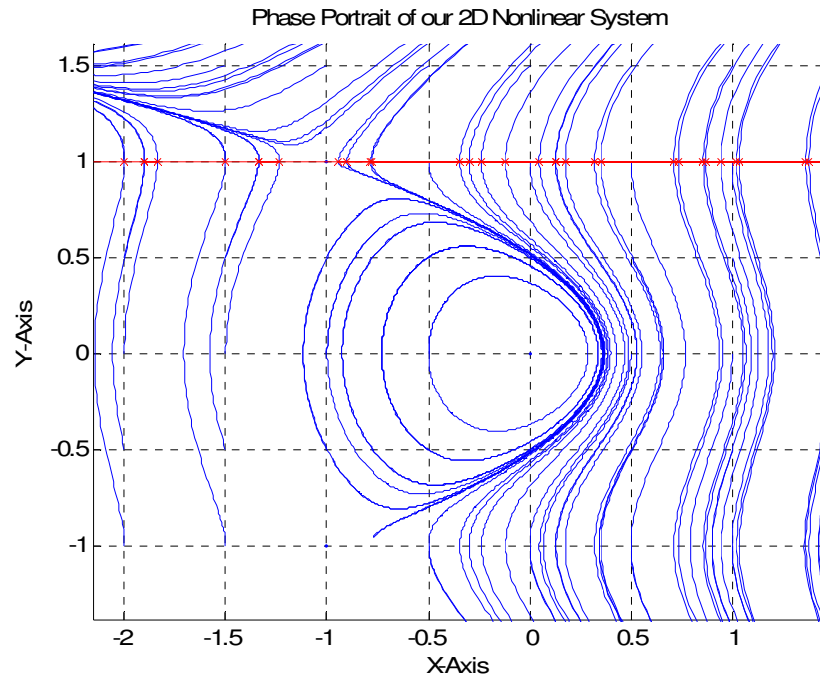


Figure 3.4. Poincare Line

The algorithm can not find overlapped intersection points and slides the line.

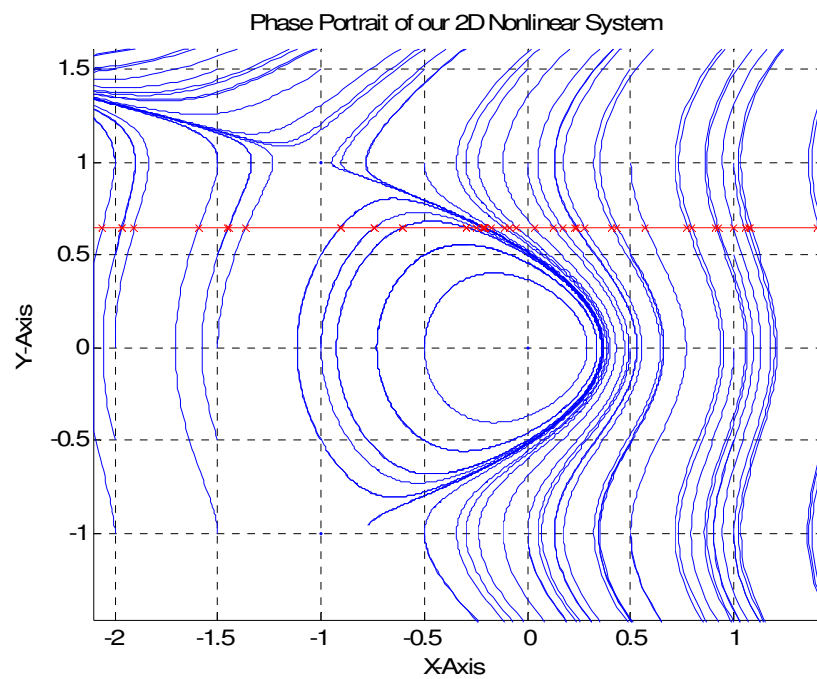


Figure 3.5. Poincare Line on Periodic Orbit

Here, the algorithm catches a periodic behaviour since the intersection points on the Poincare line are close enough.

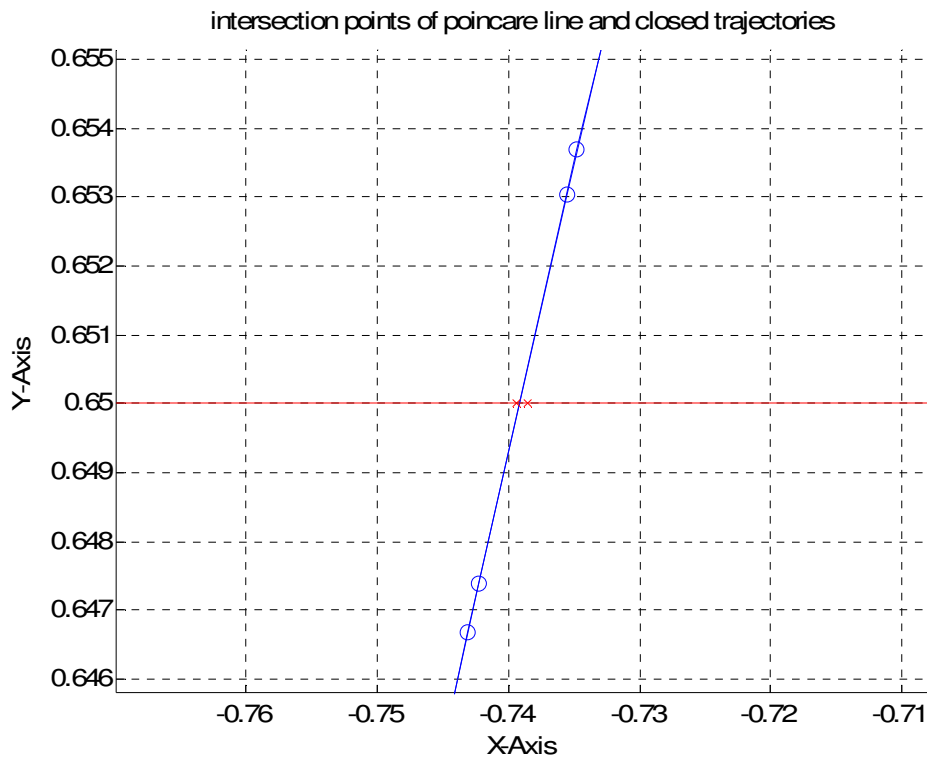


Figure 3.6. Intersection Points of Poincare Line

After all trajectories are checked, there are 3 possibilities we can find out:

- 1- There is no periodic behaviour in the system.
- 2- There is a continuum of closed orbits in the system.
- 3- There is only one closed orbit that is to say there is a limit cycle in the system.

If we find more than one closed orbits, the algorithm begins to search if any other data point which does not belong to a closed orbit stays between these orbits.

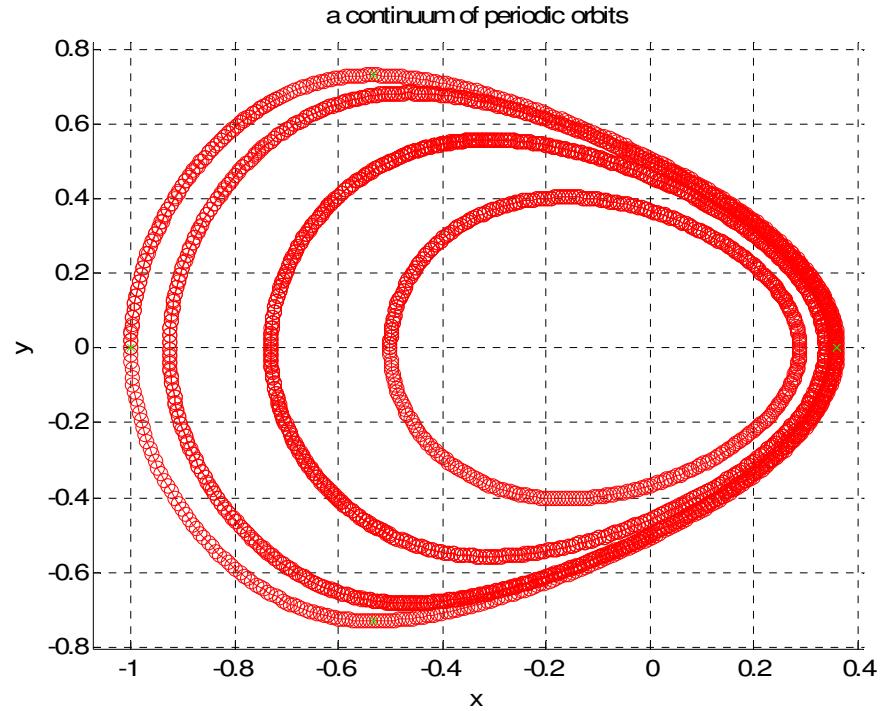


Figure 3.7. Sampled Continuum of Periodic Orbits

Note that if there is not any data point inside the innermost closed orbit, the characteristic behaviour of the system in this area can not be identified. However if the initial conditions are selected dense enough it is assumed that the continuum covers the whole area bounded by the outermost orbit.

If the algorithm fails to detect the existence of continuum of periodic orbits or if the algorithm has already found only one closed trajectory then it is concluded that here exists a limit cycle.

Example:

Consider the phase portrait in Figure 3.8.

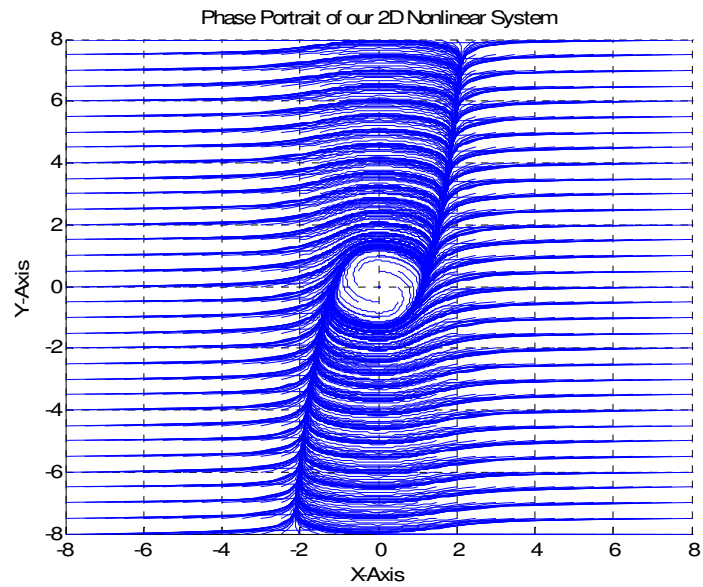


Figure 3.8. Phase Portrait of a System with a Limit Cycle

Only one closed orbit is detected as shown below.

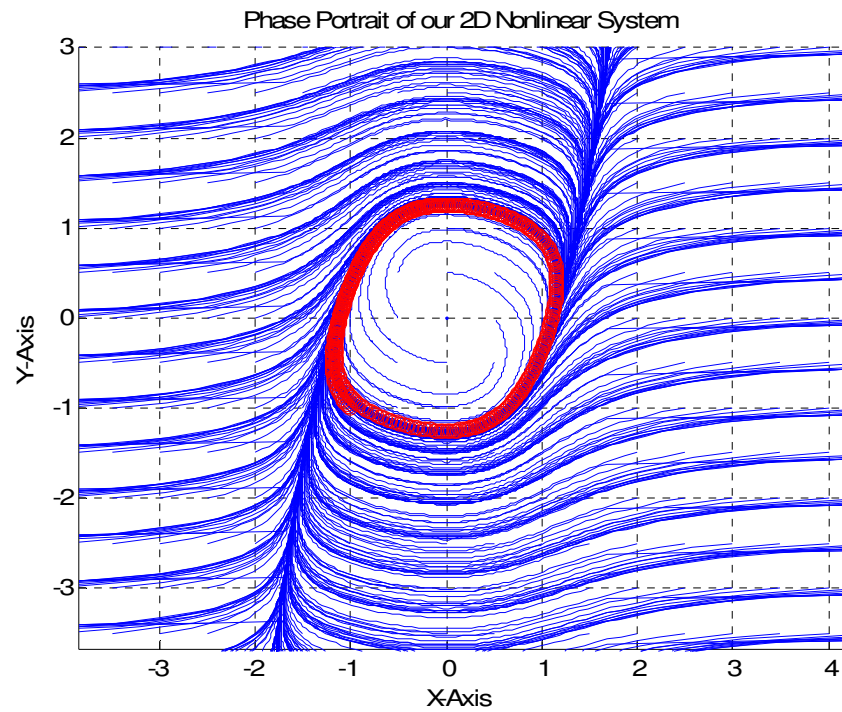


Figure 3.9. Limit Cycle in the Phase Portrait

Now, the stability of the limit cycle is asked. Any one point in the limit cycle (in our thesis the most right one) is found and the vicinity of that point is investigated. The closest points both in the outwards direction and inwards direction are found. The distance between these points and the reference point is compared with the distance between the last points in their trajectories and the reference point. If these distances become smaller, then the neighbour trajectories in the corresponding area converge to the limit cycle and hence form the basin of attraction of the limit cycle. If both distances become bigger, then the identified limit cycle is unstable. The limit cycle is said to be semi-stable if one distance gets bigger while other gets smaller.

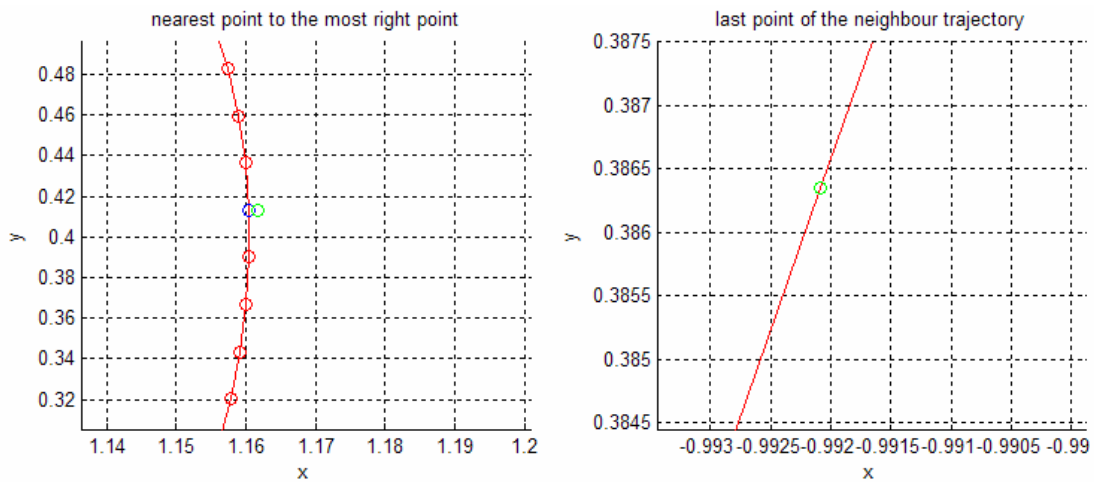


Figure 3.10. Limit Cycle Stability Analysis

In this example, the last point of the trajectory comes so close to the neighbour point that it nearly is on the limit cycle itself. Hence, it is stable in the outer region of the limit cycle.

Note that there always is a risk that due to the excess of data points the algorithm may identify a continuum of closed orbits instead of a limit cycle.

3.3. Identification of Exit Boundary Segments

To identify the basin of infinity for the researched dynamical system, we first need to find from where our system leaves the phase portrait. Afterwards we need to distinguish which trajectories tend to reach infinity from which side of the region of interest.

First a rectangular shaped frame is set onto the phase portrait.

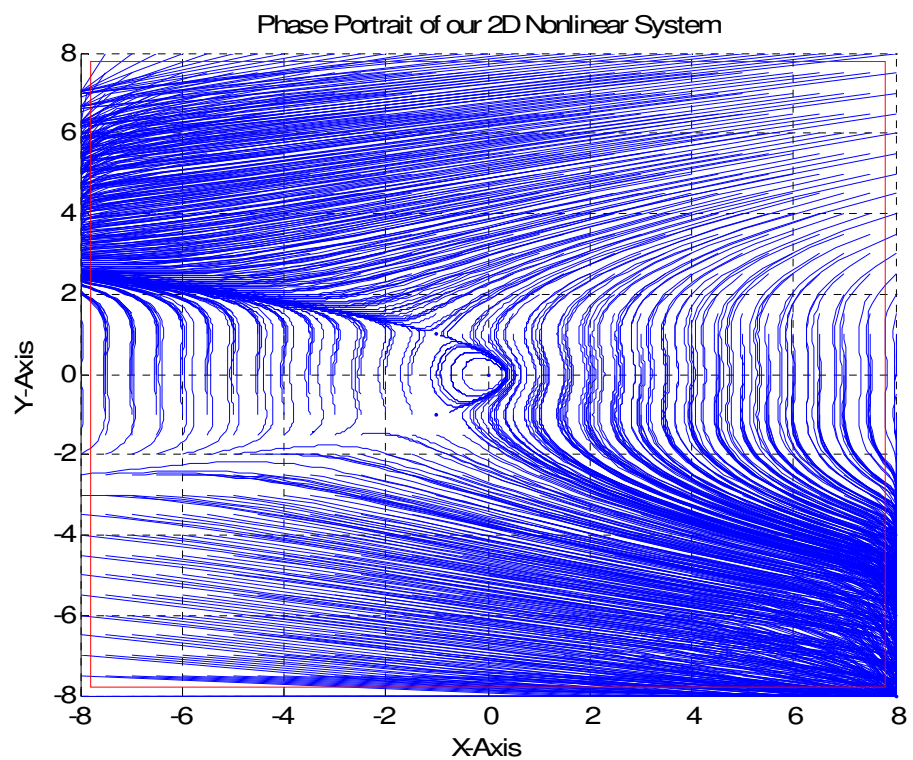


Figure 3.11. Phase Portrait Example for Exit Boundary Identification

Then, the intersection points of the trajectories and this frame are found.

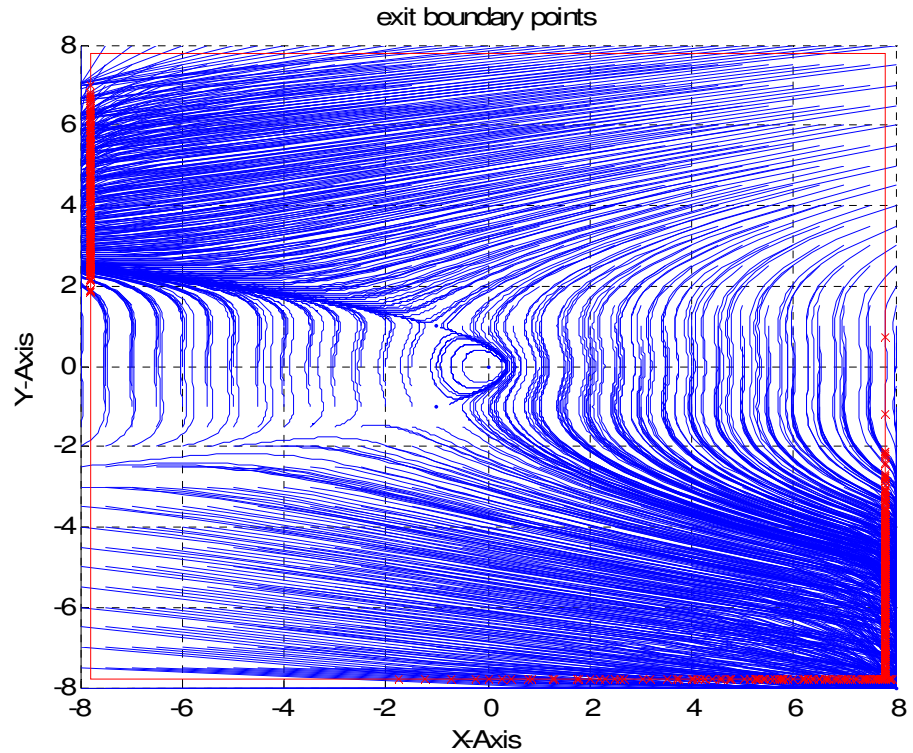


Figure 3.12. Exit Boundary Points

In this example, there are two main exit boundary segments. To assign each trajectory to one of these segments, we first need to find the “eye” of these segments, which represents where the trajectories are most dense.

This is done by kernel regression and then by finding the local peaks as the main exit boundary points.

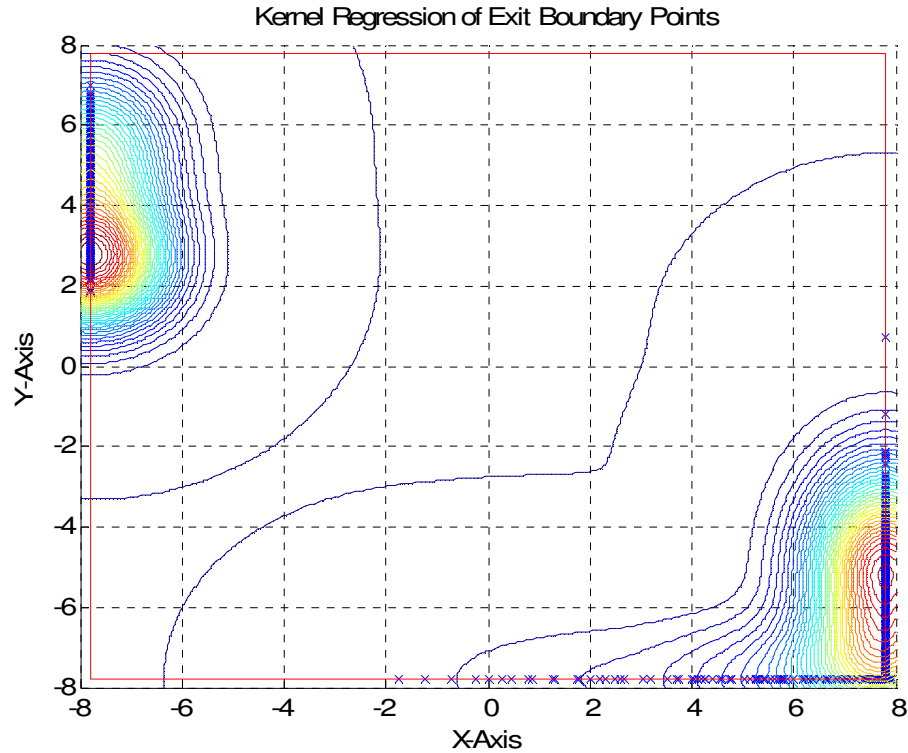


Figure 3.13. Kernel Regression of Exit Boundary Points

Then all trajectories are divided and assigned into two groups according to the distances to the eyes.

3.4. Flame Expansion Algorithm

This algorithm plays a central role in identification of basins in this thesis. After finding the equilibrium points, exit boundary segments and closed orbits, we have to estimate how the effects of those phenomena are spread along the phase space. We developed a flame expansion algorithm. The main logic behind this algorithm is similar to the skeletal transformation, a technique used in image processing to extract the skeletal information of the subject by its body image.

Consider the whole phase space as an untouched area and the cores of invariant sets as flames. Assign each different set a different type of flame. At each iteration, expand the flame in each set by making each neighbour point an active flame of the same type. Afterwards, make the already expanded flames “burnt”. Burnt areas do not transmit the flame to their neighbourhood and just stand still. If any active flames of the same type meet each other, they become “burnt” and stops burning. If any two active flames of different types meet each other, they immediately form a boundary flame segment which is immobile too. Iterations are processed until all the untouched areas become burnt points and the whole phase space is covered by boundaries of basin of attractions.

Example:

Below, 3 different type of invariant sets are shown. Each iteration makes the flames wider and when they meet each other, they create a boundary and flames stop expanding in that direction.

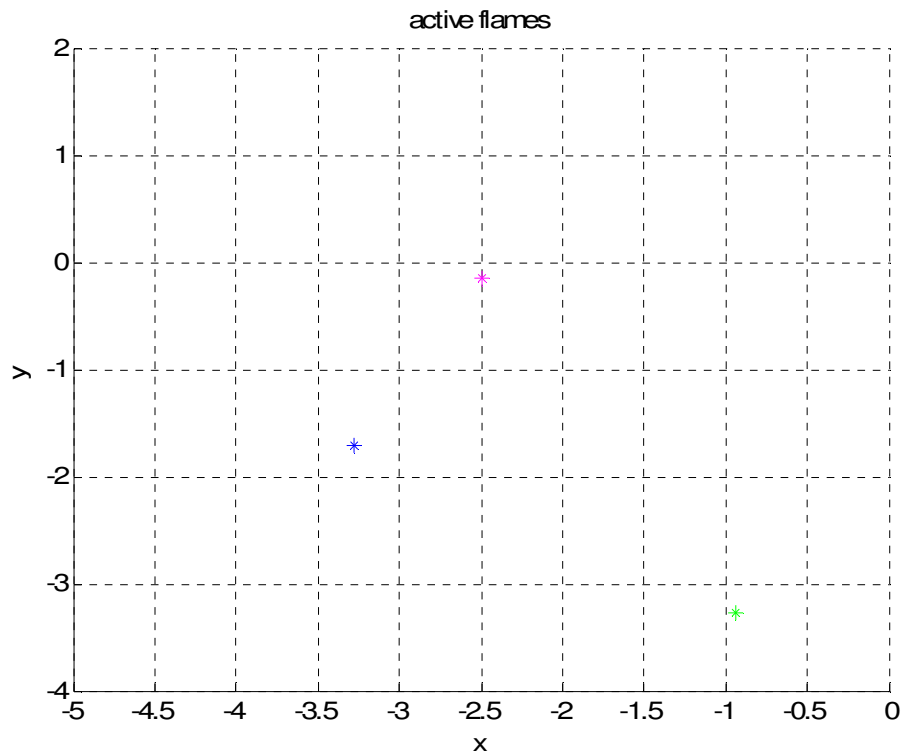


Figure 3.14. Three Different Kind of Flames

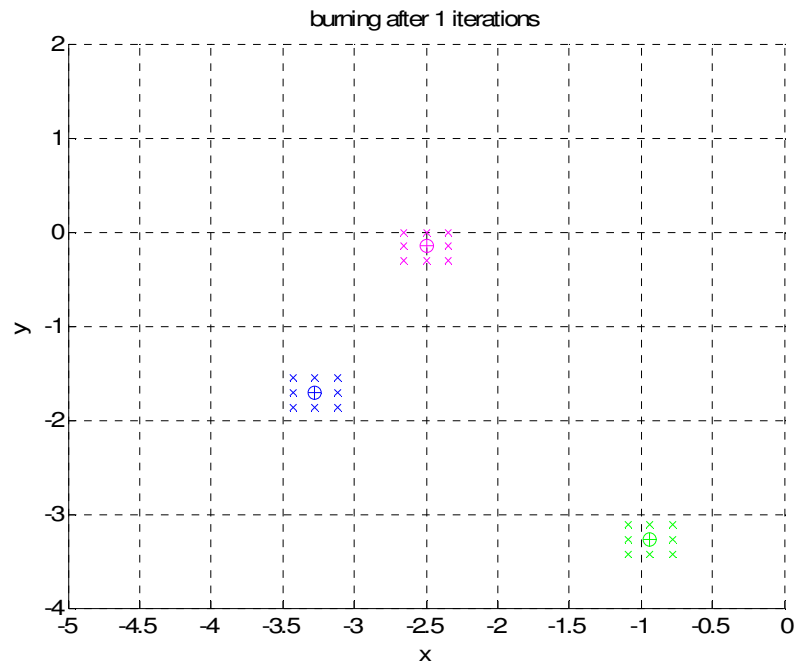


Figure 3.15. Expansion of the Flames after 1 Iteration

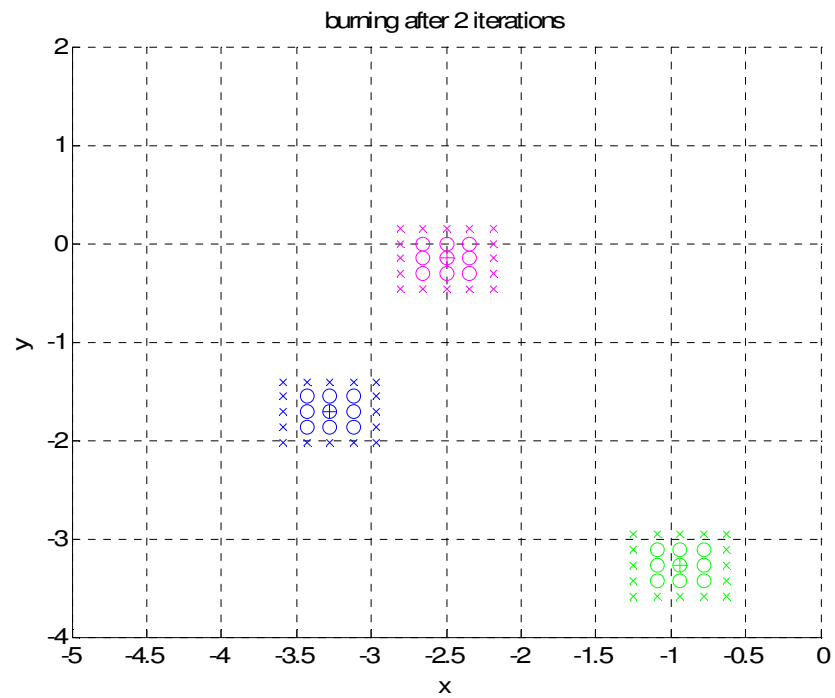


Figure 3.16. Expansion of the Flames after 2 Iterations

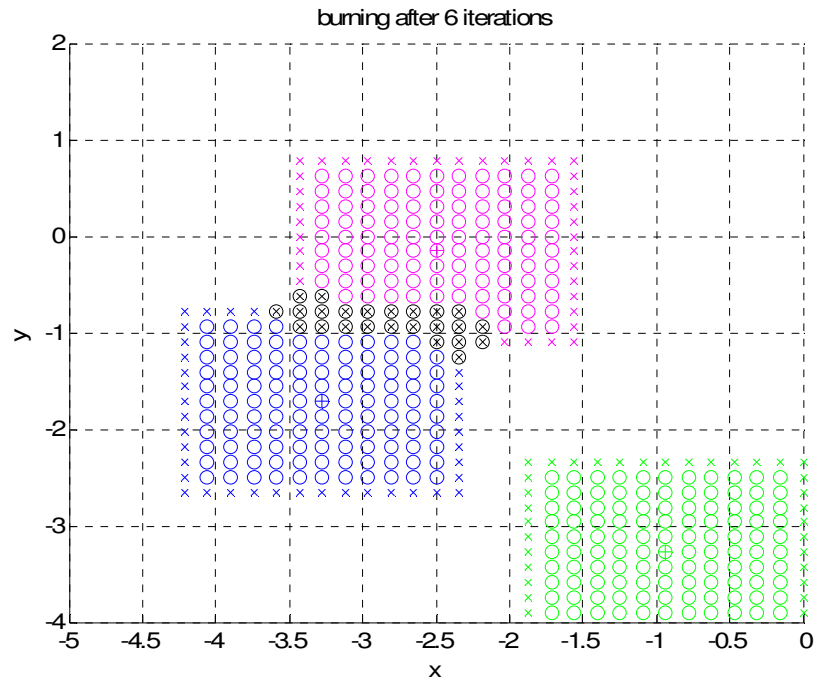


Figure 3.17. Expansion of the Flames after 6 Iterations

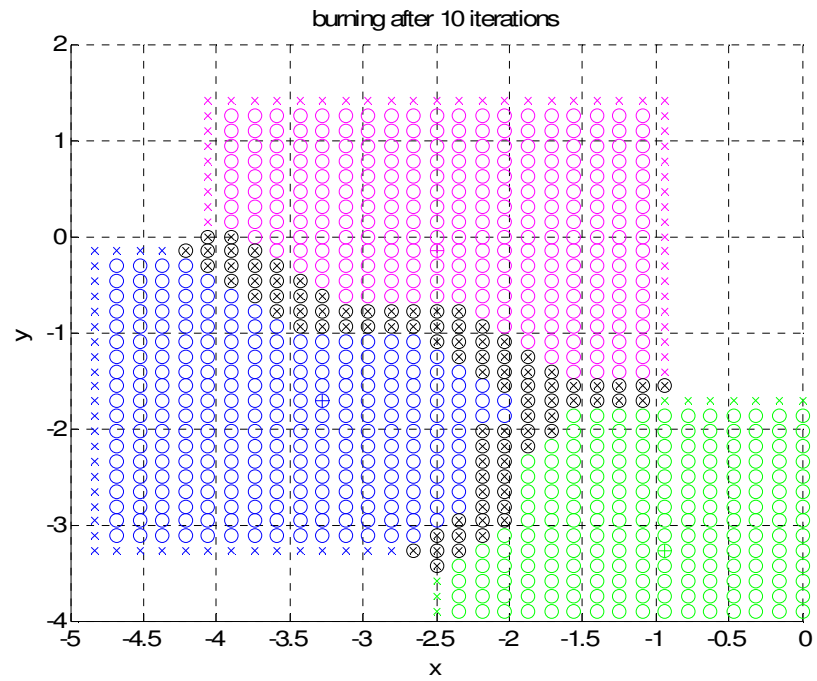


Figure 3.18. Expansion of the Flames after 10 Iterations

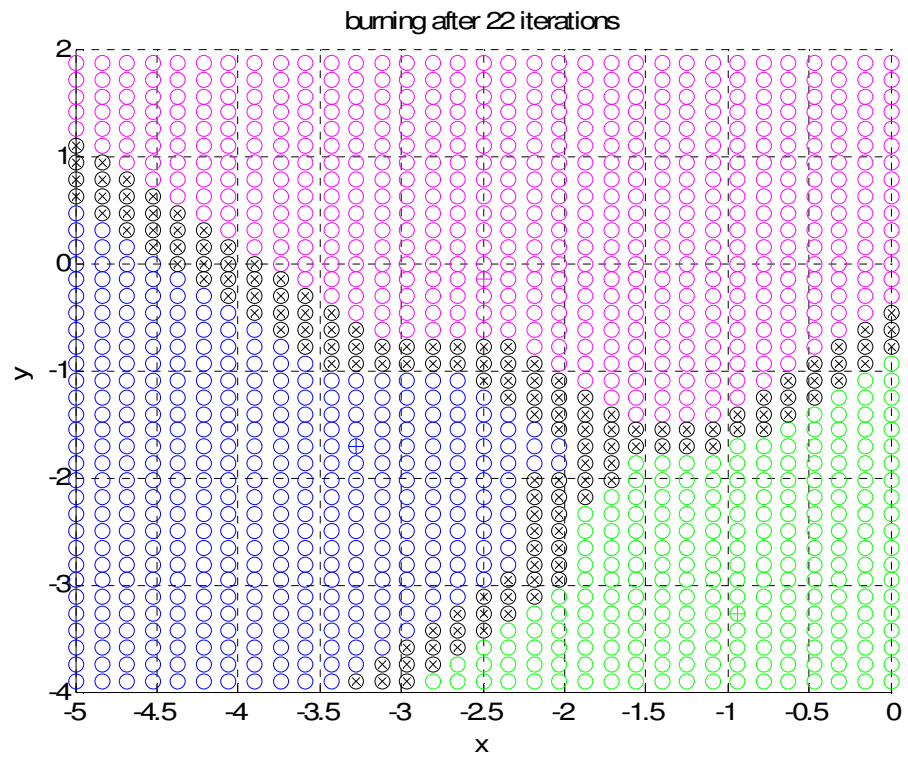


Figure 3.19. Expansion of the Flames after 22 Iterations

4. COMPLEMENTARY WORK AND DIFFERENT APPROACHES

4.1. Image Processing Filters

Although we are mainly focused in this thesis on the basin description and representation, the next step in this research area would be controlling the dynamics inside the basins. As a contribution and as a preliminary work, we used image processing techniques on the given system data to obtain a more regularized picture.

Idea: Since both the differential equations and the colored picture data can be seen as vector fields, apply the image processing techniques and filters to the dynamical equations.

We consider the whole phase portrait as an noised image and if we use specific image processing techniques, like sharpening or deblurring filters, we can obtain a “smoother” or “better” picture that shows us the long term behaviours clearer. Although the idea is original, selecting the right filter or even designing an appropriate one is beyond the duty of this thesis and that is why this work is limited to one filter only.

We used the unsharp filter created as

$$\frac{1}{\alpha+1} \begin{bmatrix} -\alpha & \alpha-1 & -\alpha \\ \alpha-1 & \alpha+5 & \alpha-1 \\ -\alpha & \alpha-1 & -\alpha \end{bmatrix} \quad (4.1)$$

where α is chosen as 0.2 .

The sharpening effect of the filter on the photography can be seen below:



Figure 4.1. Effect of the Sharpening Filter

To use this filter, the phase portrait has to be defined as a image data. The flow vector at each data point is treated as an “RedGreenBlue” true color image pixel. Each independent component of the vector assigned for the red, green or blue intensity of the pixel. Since in this thesis this technique is applied only on 2D systems, we added an artificial constant to each data point as a third dimension which represent the blue intensity. The data range for image processing is between 0 and 1. After rescaling the new 3D-vectors so that all the components are in the range (0-1), the phase portrait was ready to be processed by a filter.

Example:

Assume that,

- there is a flow vector, $F = \begin{bmatrix} -0.4 \\ 1.5 \end{bmatrix}$ on one of the data points
- the phase space has the biggest flow in the negative direction on $\begin{bmatrix} x^{*-} \\ y^{*-} \end{bmatrix} = \begin{bmatrix} -0.8 \\ -0.1 \end{bmatrix}$ and the biggest flow in the positive direction on $\begin{bmatrix} x^{*+} \\ y^{*+} \end{bmatrix} = \begin{bmatrix} 1.2 \\ 1.7 \end{bmatrix}$

Since we want to rescale the whole phase space to 0-1 range, we assigned the most negative flow to “0” and the most positive flow to “1” at each direction. The other flows are adjusted according to this rescaling, that is to say

$$F_{scaled} = \begin{bmatrix} (-0.4 + 0.8)/(0.8 + 1.2) \\ (1.5 + 0.1)/(0.1 + 1.7) \end{bmatrix} = \begin{bmatrix} 0.2 \\ 0.89 \end{bmatrix}$$

After adding an artificial 0.5 as a third dimension we have a true-color image pixel of $\begin{bmatrix} 0.2 \\ 0.89 \\ 0.5 \end{bmatrix}$ at the data point in the example. This pixel is sharpened by the filter described by equation 4.1.

One of the harder tasks was to decode the pixel data to flow vector data after the filtering process. The new pixel was transformed to a new vector by rescaling again and removing the third dimension. However, at the end of this vector there may be no data point so that a new trajectory can be constructed. An algorithm is developed which generates a rectangular so that the end of our new vector stands on the center. Then, the number of neighbor data points which are also inside the rectangular are checked. If there is sufficient amount of data points, their weight on our new data point is computed and the new flow vector is found. The sufficiency rule is chosen in such a way so that there is at least one data point in each quadrant around the new data point.

Example:

The red data point in figure 33 is where the new vector flow will be computed. The selection of the neighbour points is determined by the red rectangular. In this example, there is at least one data point in each quadrant around the red point. So, the rectangular is not expanded anymore to catch new neighbours.

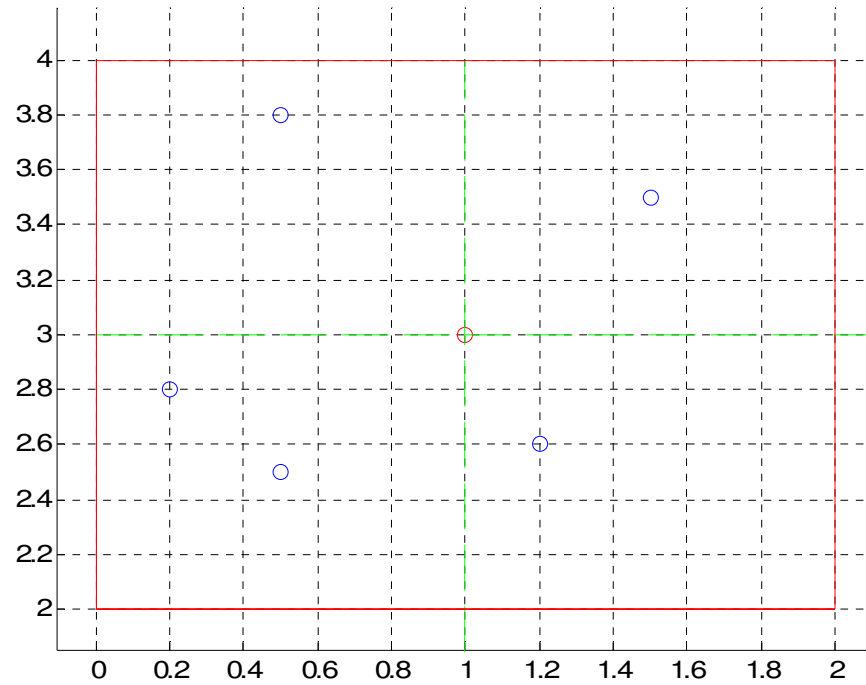


Figure 4.2. Choosing the Neighbour Points

The new flow vector is computed according to:

$$\zeta^* = \frac{1}{k} \sum_{i=1}^k \left(\frac{\frac{1}{k} \sum_{j=1}^k \|\zeta_j - \zeta^*\|}{\|\zeta_i - \zeta^*\|} \zeta_i^* \right) \quad (4.2)$$

where,

ζ^* : our new data point after filtering (the red point above)

ζ : the neighbour data points (the blue points above)

ζ^* : the flow vector at the neighbour data points : $F(\zeta) = \zeta^*$

ζ^* : the estimated flow vector at our new data point : $F(\zeta^*) = \zeta^*$

According to equation 4.2, the effect of the neighbours weakens as its distance increases. So, close neighbour vectors have a stronger role in determining the new flow vector.

After the new flow vector is computed, another new data point is found at the end of this vector and the processes above are reiterated until the trajectory completed.

In figure 4.3., the result of the whole algorithm is shown. The green lines indicate the original trajectories and the red lines indicate the filtered trajectories. Note that in some cases, especially in the closed orbits, the algorithm changes the trajectory so much that it loses its characteristic behaviour.

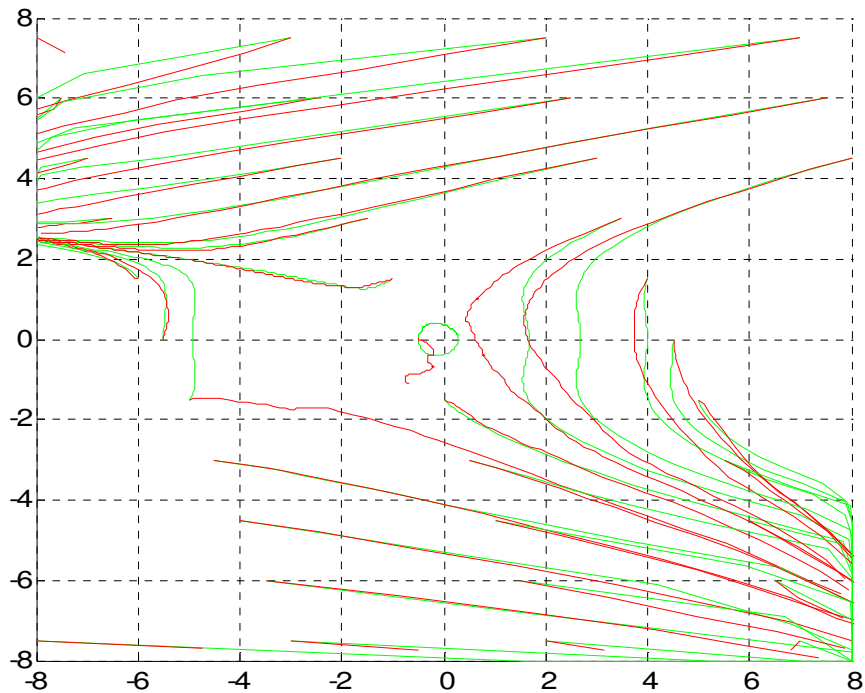


Figure 4.3. Phase Portrait after Filtering

However, it is also observed that the transformed trajectories now have a rougher shape and the path of the trajectory, that is to say where it will converge, is seen clearer.

By choosing other filters, the dynamics of the system can be simplified without changing the characteristic basins and invariant sets. Designing such a filter and researching if it can be improved by making it to dependent to some statistical information obtained from the dynamical system, is left as an open problem.

4.2. The Backbone Extraction

Idea: Once the exit boundary segments are found, if the trajectories tend to form an asymptote towards the exit boundary, then this main stream can be extracted by using variable kernel regression.

First, a kernel function is placed on each data point to find the local peaks which should show the trace of the backbone. However this approach obviously enclosed unwanted peaks which are formed when data points in a trajectory are very close each other that is to say the trajectory flows slowly enough.

After many trials, two modifications to our regular kernel function, which we used through the whole thesis, are made:

- Each kernel function's bandwidth varies according to the average distance of the data point to neighbours in its trajectory.
- The heights of the kernel function are held constant while the volumes vary according to their bandwidth.

After these modified kernels are processed on a periodically sampled group of data points, the local peaks are found.

Now, some of those local peaks are standing on the backbone of the exit boundary segments. To find which, we first determined the closest trajectory to the core of the exit boundary segment. Then this trajectory is back-traced and all the peaks which are close enough to the trajectory is activated. In other words, it is checked if this trajectory passes through the inside of the projection of cross section that is cut from the $1/e$ of the peak. If it does, then that peak is marked.

At last, all the marked peaks are used to estimate a second order polynomial which is chosen to represent the backbone of the exit boundary segments.

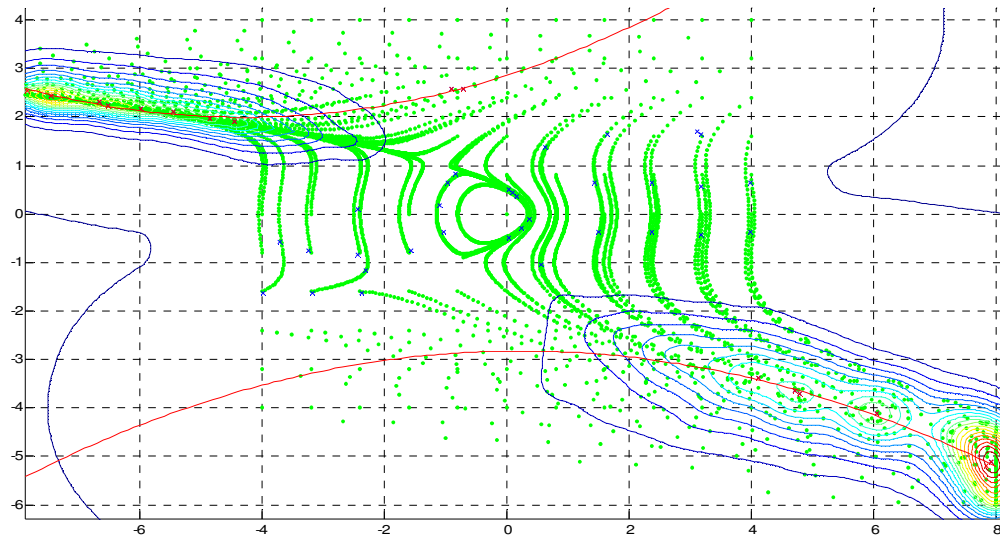


Figure 4.4. Backbones

The activated peaks are marked red. Blue crosses are other local peaks which does not have any role on determining the backbone.

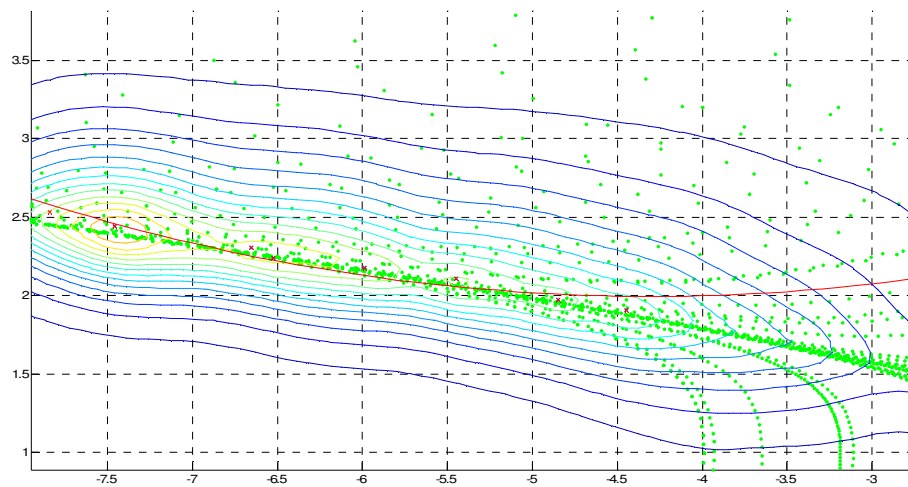


Figure 4.5. Backbone Estimation from the Activated Peaks

The backbone algorithm may be used with the other basin of attraction estimation algorithms we introduced to make a more detailed interpretation for the long-term behaviour of our nonlinear system.

4.3. Preliminary Work for 3-Dimensional Systems

Due to time limitations and more problematic situations, we will not be able to extend all the algorithms comprehensively to three dimensional systems. In addition of more complicated behaviour types and invariant sets, we also lose our visualization advantage of Kernel functions in 2-dimensional systems. However an introduction has been made with modified versions of the algorithms which are proposed in the thesis.

Our results will be presented over the following system and initial conditions.

$$\begin{aligned} \dot{x} &= x^3 - x & x_0 &= [-3 \quad -2.6 \quad \dots \quad 2.6 \quad 3] \\ \dot{y} &= -2y & y_0 &= [-3 \quad -2.6 \quad \dots \quad 2.6 \quad 3] \\ \dot{z} &= -2z & z_0 &= [-3 \quad -2.6 \quad \dots \quad 2.6 \quad 3] \end{aligned}$$

The phase portrait of this system is shown below.

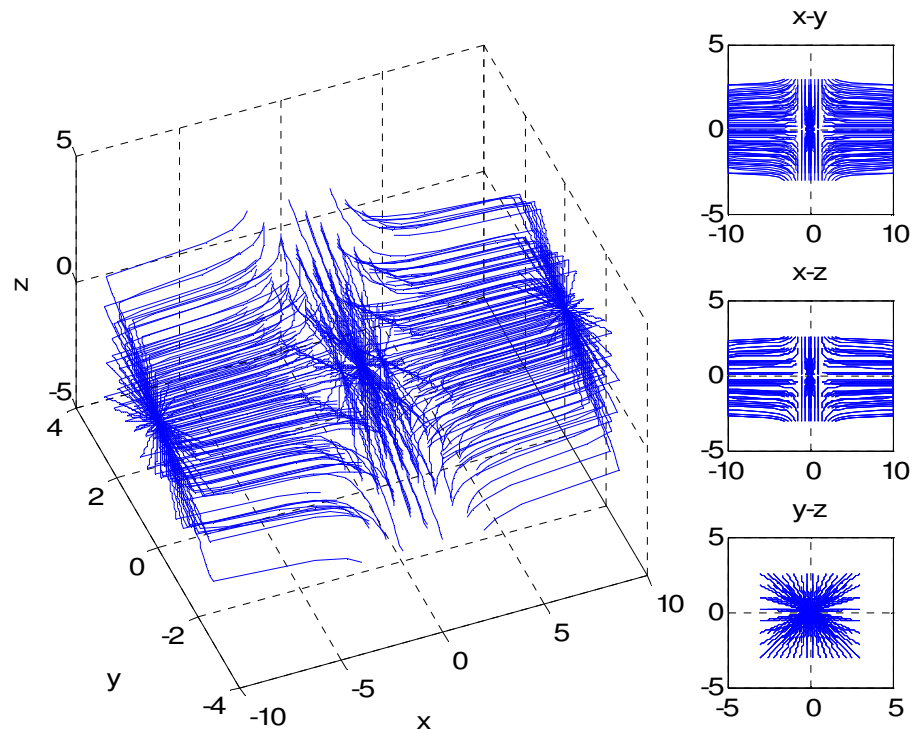


Figure 4.6. Phase Portrait of a 3D-System

The region of interest is a cube whose center is the origin and has length of edges of 4.

1- First the enter and exit regions are computed by tracing each trajectory and finding the intersection points on the surfaces.

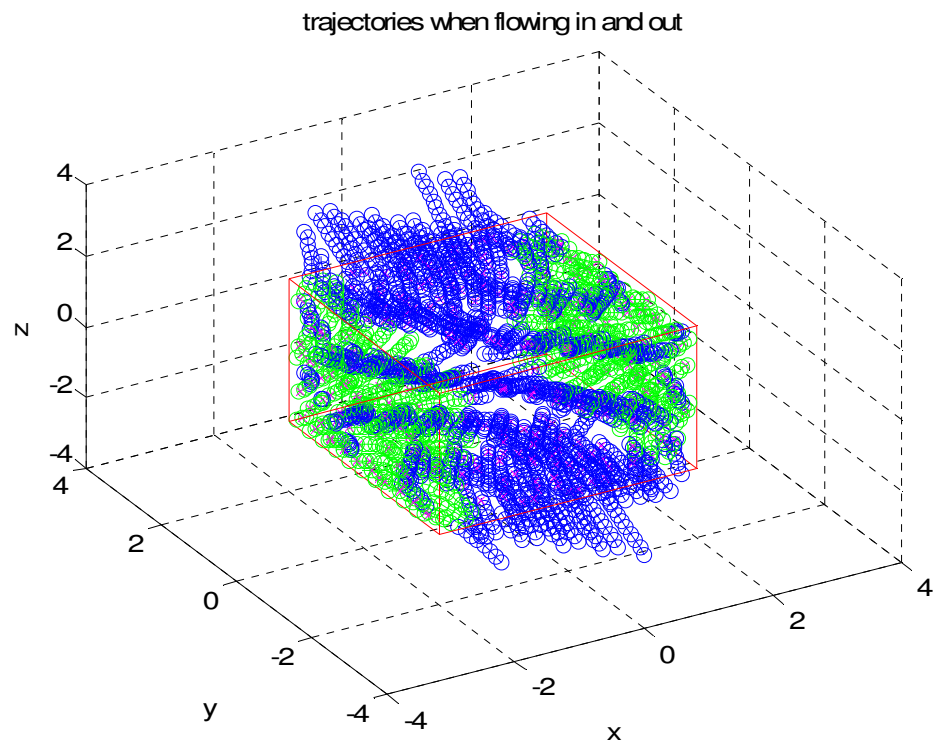


Figure 4.7. Trajectories Entering and Flowing Out

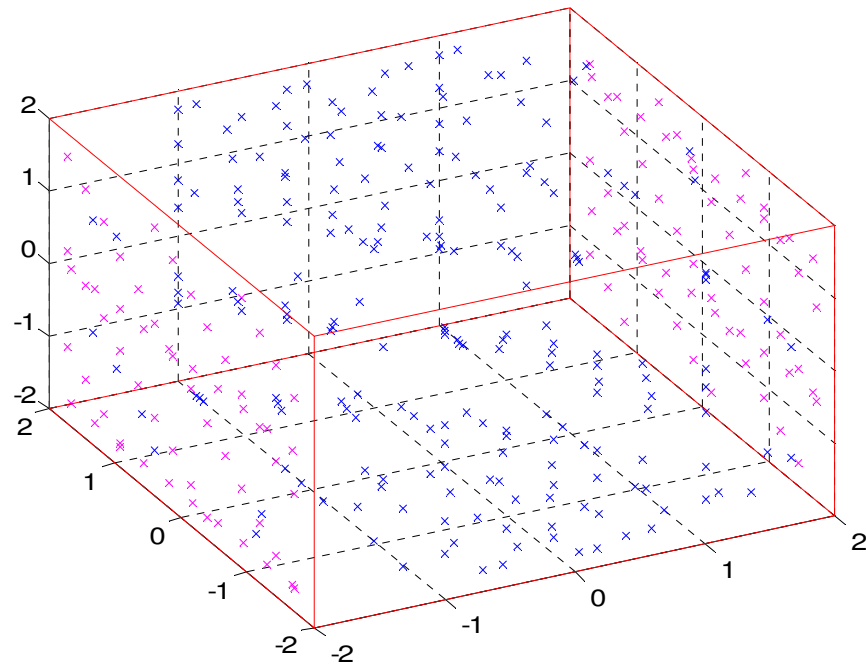


Figure 4.8. Exit and Entrance Points on ROI

2- The flame expansion algorithm is applied to a sampled data on each surface to determine the main exit- and enter- regions.

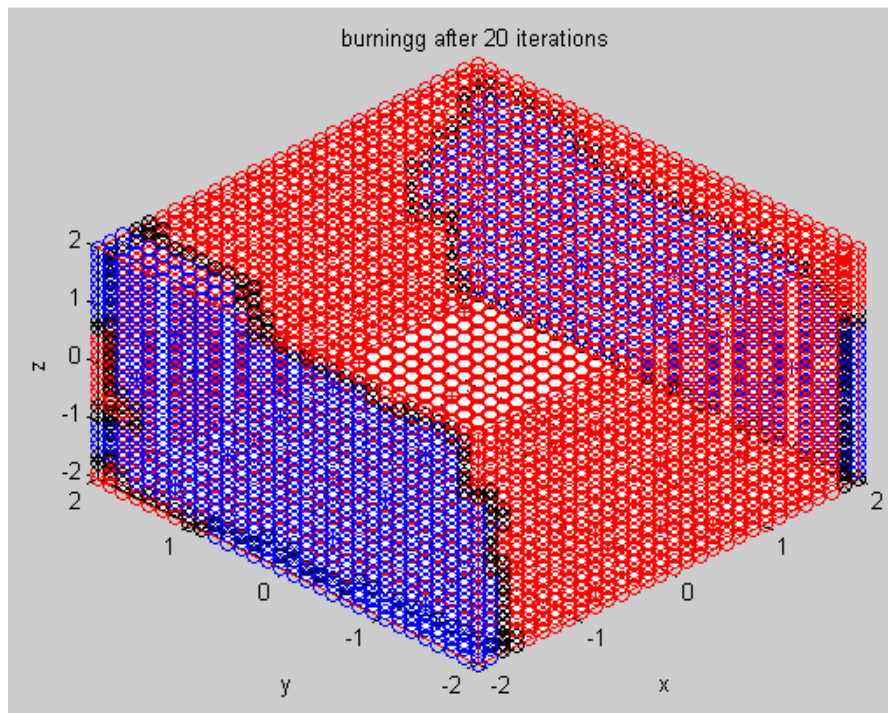


Figure 4.9. Flame Expansion on Surfaces of ROI

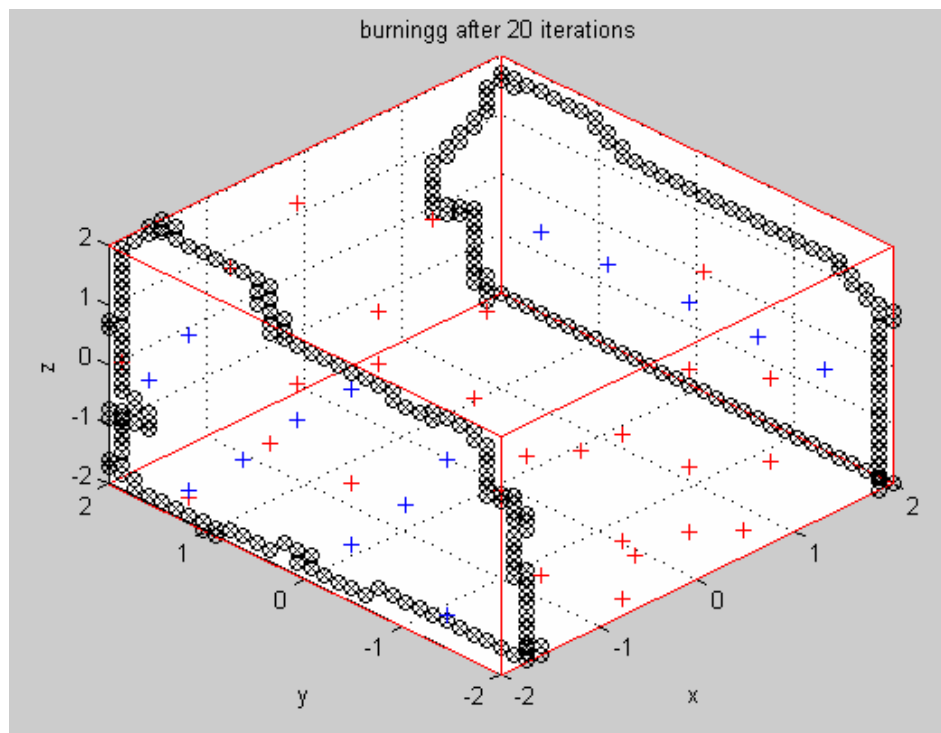


Figure 4.10. Boundaries on the Surface

3- The stable equilibrium points are computed with the help of a direct extension of the algorithm for 2-dimensional systems. 3-dimensional Kernel functions are used to estimate the location of equilibrium point candidates. However, in this example the saddle points at $x_1^* = [1 \ 0 \ 0]$ and at $x_2^* = [-1 \ 0 \ 0]$ have planary stable manifolds and the trajectories that start in this manifold cause the algorithm to recognize saddles as attractive equilibrium points.

4- At last the flame extension algorithm is extended to 3 dimensional data. Expanding cubes are used instead squares. As in 2-dimensional version, the boundaries are formed when 2 different type flames encounter.

However we did not use parametric regression to represent the basins of attraction due to the complexity of the nonlinear models and left the question open.

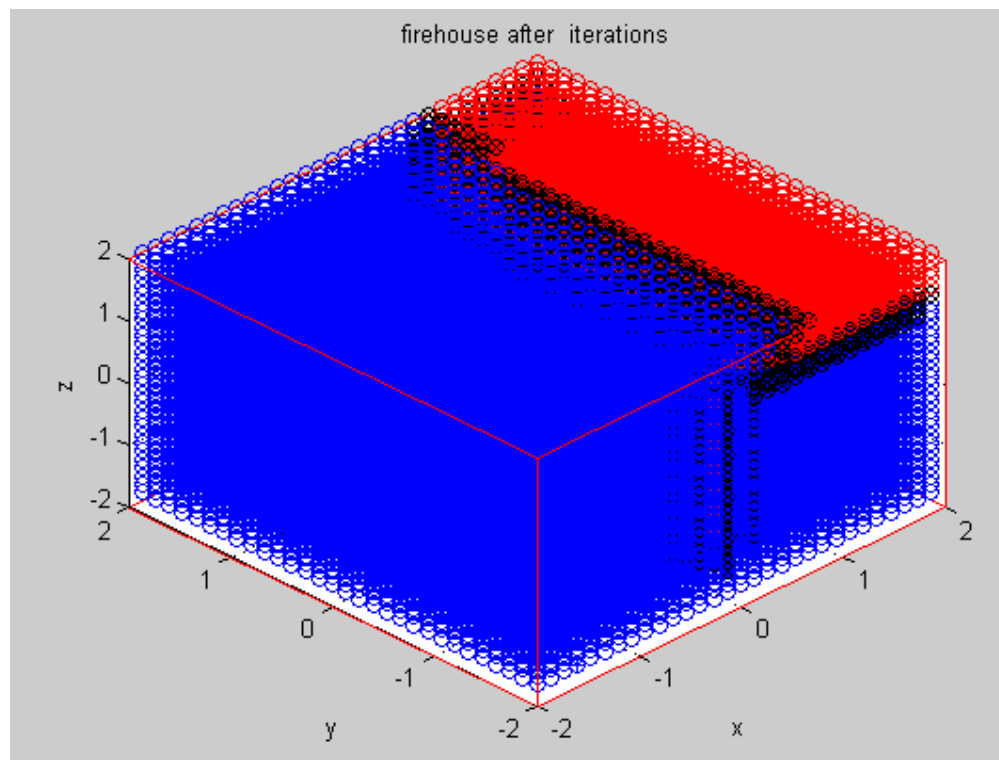


Figure 4.11. Flame Expansion inside the ROI

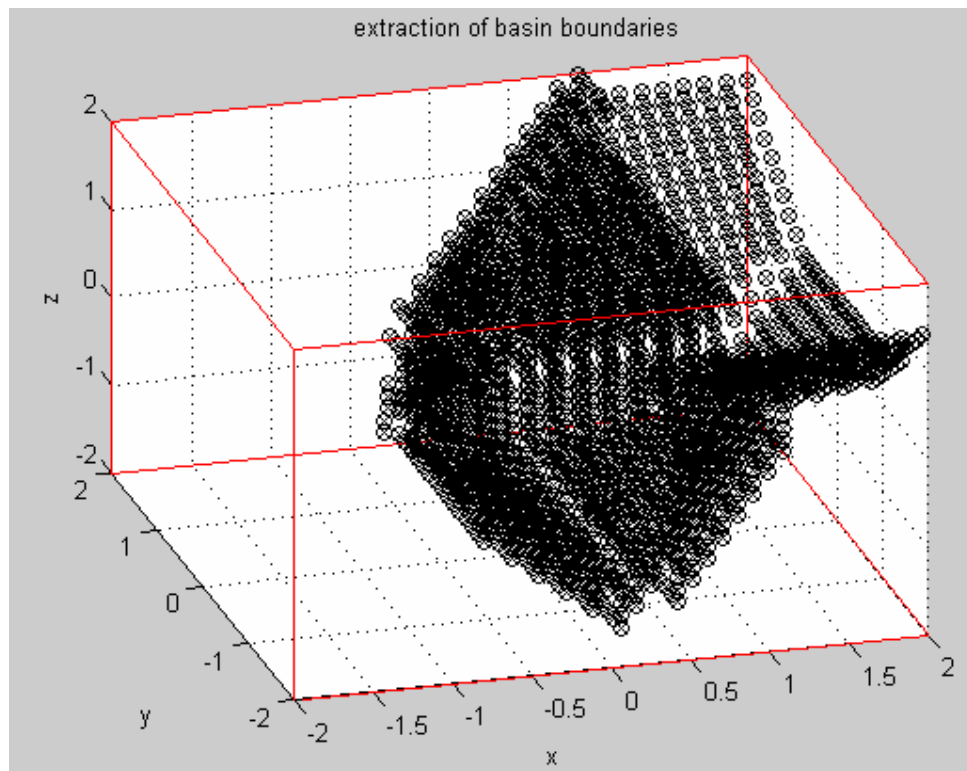


Figure 4.12. Boundary of Basin of Equilibrium Points

5. SIMULATION RESULTS

The common parameters

- Simulation time: 10 seconds
- Sampling time : 0.02 seconds
- Ordinary differential equations solver algorithm: Bogacki-Shampine algorithm
- Kernel Regression are computed at 200x200 grid with a bandwidth

matrix $H = \begin{bmatrix} h & 0 \\ 0 & h \end{bmatrix}$ where h is taken from researcher

Models used for nonparametric regression:

1- $y = ax^2 + bx + c$

2- $y = ax^3 + bx^2 + cx + d$

3- $ax^2 + bxy + cy^2 + dx + ey + f = 0$

4- $ax^2y^2 + bxy^2 + cy^2 + dx^2y + ex^2 + fxy + gx + hy + i = 0$

Unless mentioned otherwise, all the parameters asked to the user is selected as default:

- The bandwidth constant for kernel estimation on the boundaries = 1
- The number of final points that will be checked on each trajectory in order to detect stable equilibrium point = 70
- The bandwidth constant for kernel estimation on attractive points = 0.1
- The tolerance to be used in the detection of stable equilibrium points = average distance of data points in their trajectories
- The tolerance value to be used in the detection of periodic orbits = 0.0009
- The step size used in the search of useful poincare line = 0.1
- The grid size for the flame estimation algorithm = 100x100
- The maximum number of iterations of flame expansion to be used for basin boundary detection = 100

5.1. System I

$$\begin{aligned} \dot{x} &= y - y^3 & x_0 &= [-8 \quad -7.5 \quad \dots \quad 7.5 \quad 8] \\ \dot{y} &= -x - y & y_0 &= [-8 \quad -7.5 \quad \dots \quad 7.5 \quad 8] \end{aligned}$$

The frame constant $n=7.8$

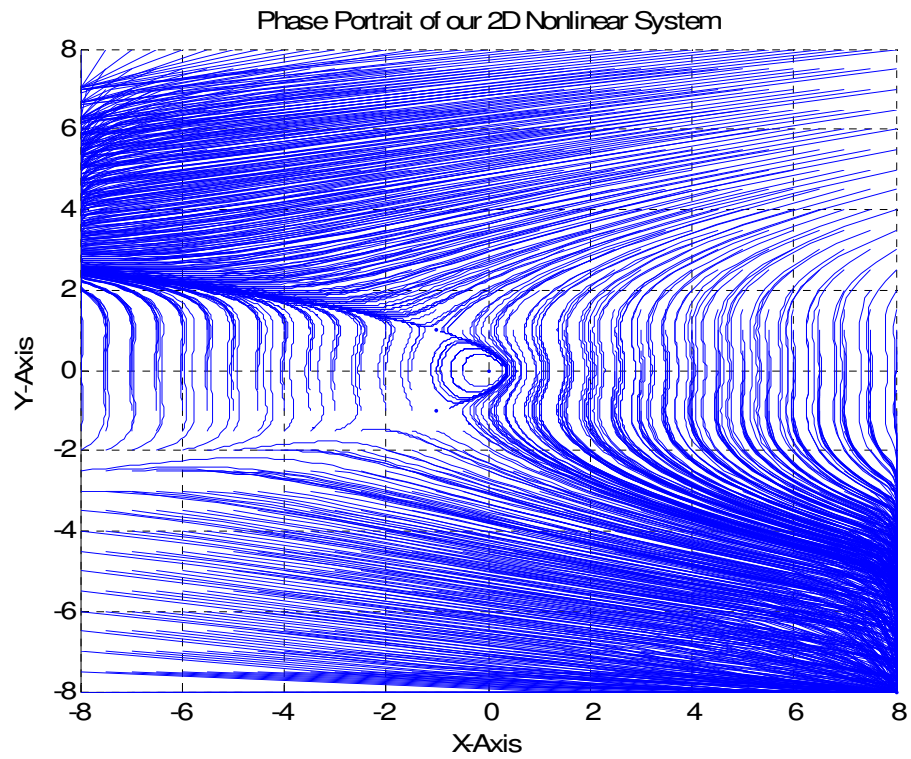


Figure 5.1. Phase Portrait of System I

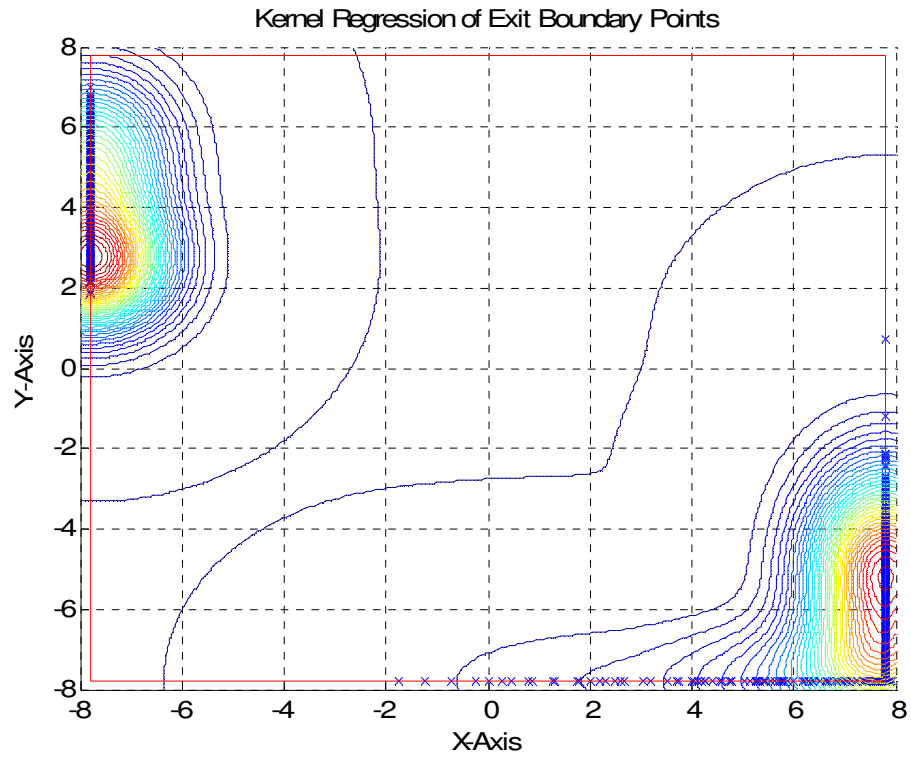


Figure 5.2. Kernel Regression of Exit Points of System I

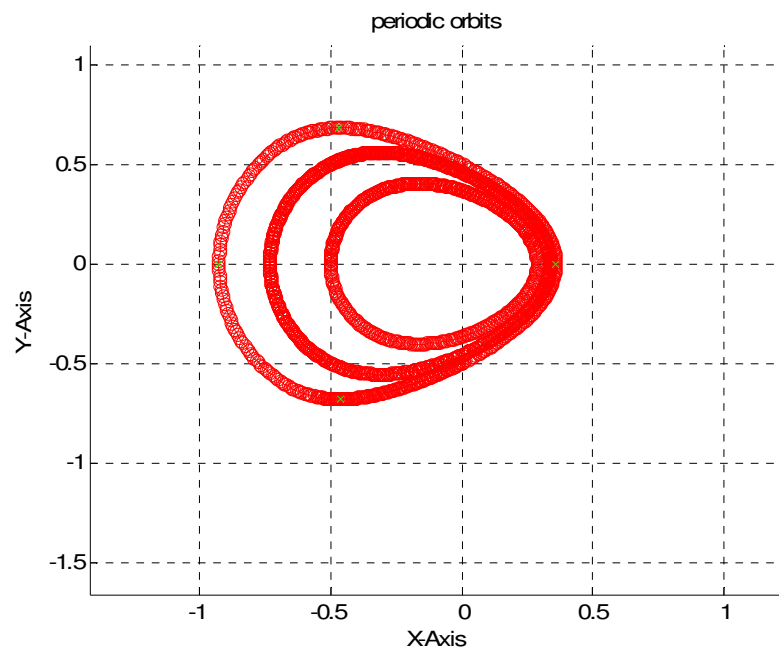


Figure 5.3. Periodic Orbits of System I

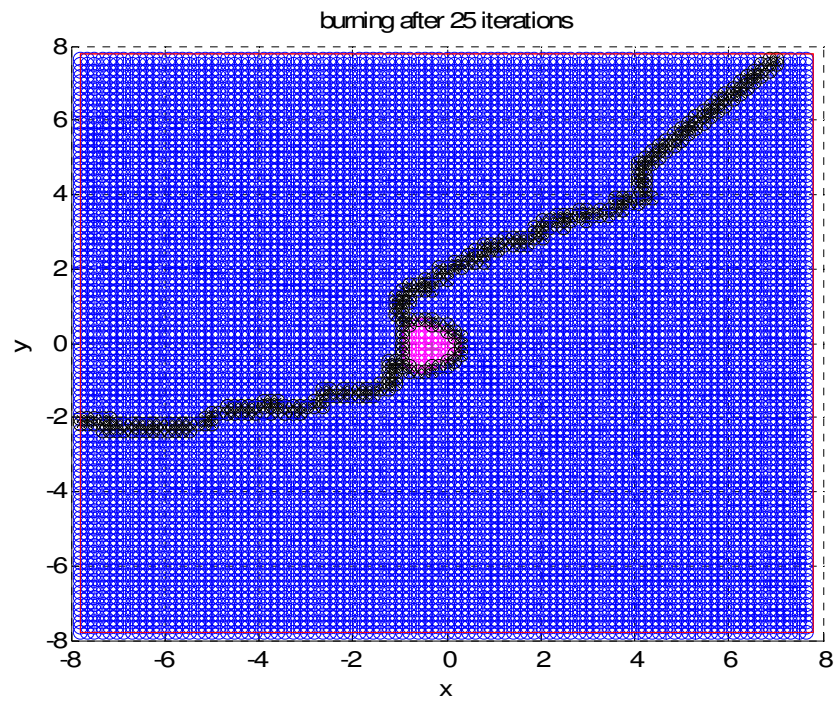


Figure 5.4. System I after Totally Burnt

Parametric regression of each invariant set with 4. model

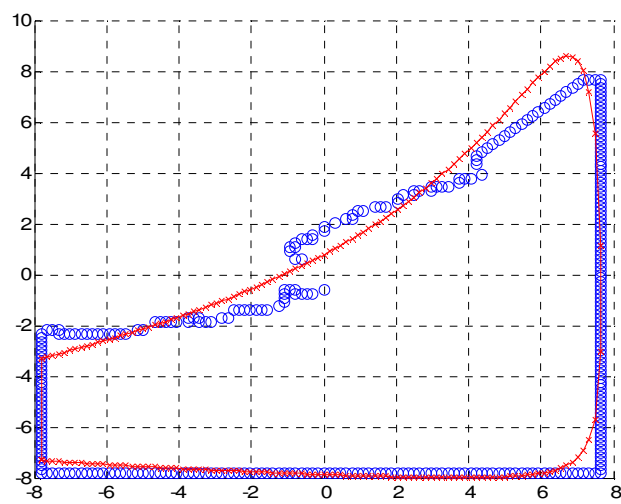


Figure 5.5. 1. Exit Basin Estimation of System I

1. parameter is $6.43738e-033$
2. parameter is $-1.34674e-031$
3. parameter is $6.70099e-031$
4. parameter is $1.06628e-031$
5. parameter is $4.91137e-031$
6. parameter is $-1.43236e-030$
7. parameter is $-3.22365e-030$
8. parameter is $4.75018e-030$
9. parameter is $-4.1137e-030$

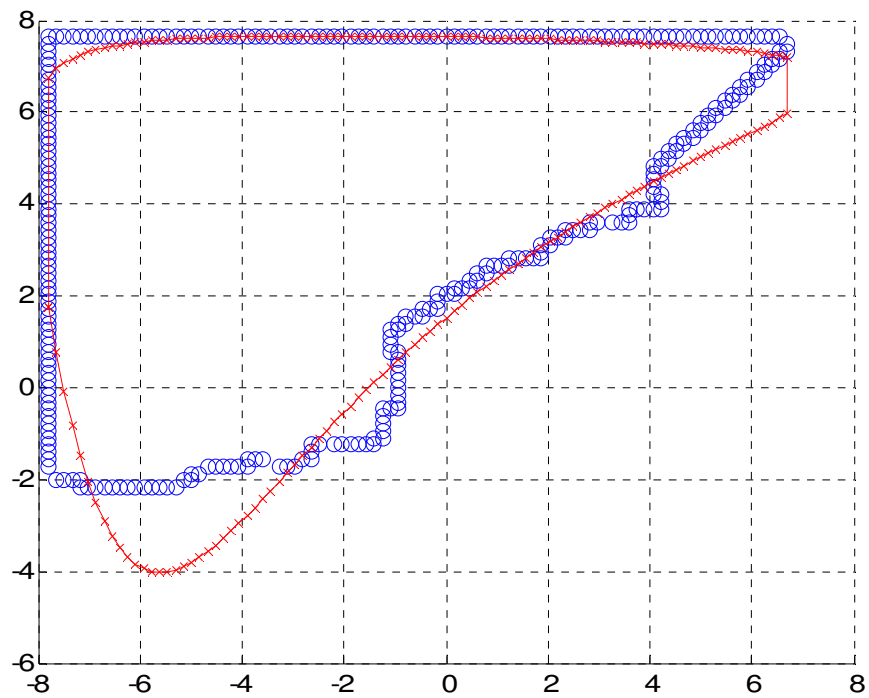


Figure 5.6. 2. Exit Boundary Estimation of System I

1. parameter is $1.89429e-028$
2. parameter is $3.3381e-027$

3. parameter is $1.72767e-026$
4. parameter is $-3.69711e-027$
5. parameter is $1.77003e-026$
6. parameter is $-4.6145e-026$
7. parameter is $1.5972e-025$
8. parameter is $-1.58487e-025$
9. parameter is $2.01516e-025$

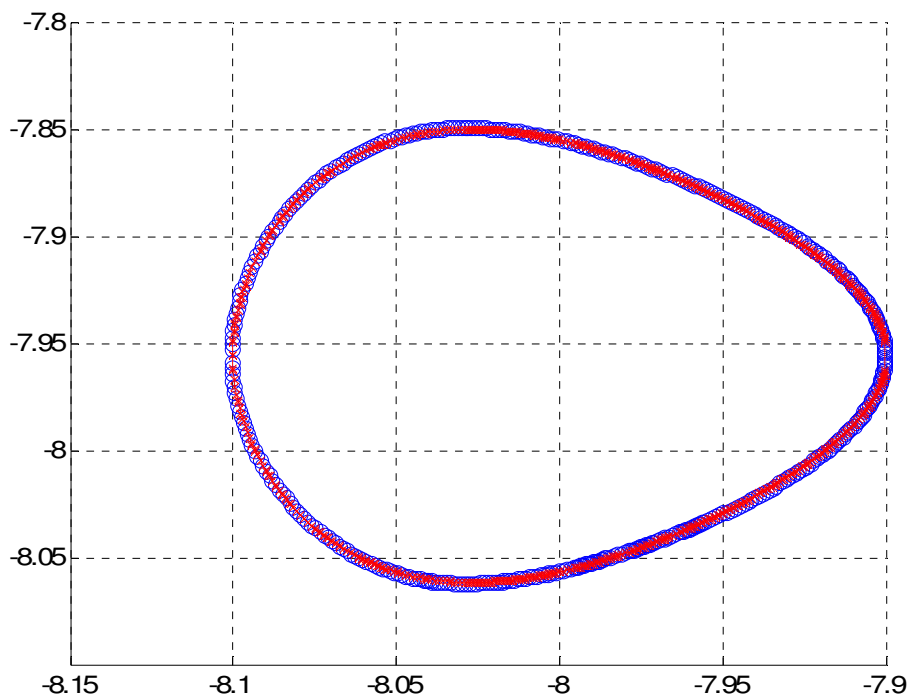


Figure 5.7. Periodic Orbit Estimation of System I

a perfect match!

1. parameter is $1.22402e-021$
2. parameter is $1.98209e-020$
3. parameter is $8.02646e-020$
4. parameter is $1.94761e-020$
5. parameter is $7.75091e-020$

- 6. parameter is 3.15381e-019
- 7. parameter is 1.25512e-018
- 8. parameter is 1.27713e-018
- 9. parameter is 5.08255e-018

5.2. System II

$$\begin{aligned} \dot{x} &= -(2 \sin x + \sin y) & x_0 &= [-8 \quad -7.5 \quad \dots \quad 7.5 \quad 8] \\ \dot{y} &= -(2 \sin y + \sin x) & y_0 &= [-8 \quad -7.5 \quad \dots \quad 7.5 \quad 8] \end{aligned}$$

The frame constant $n=3.8$

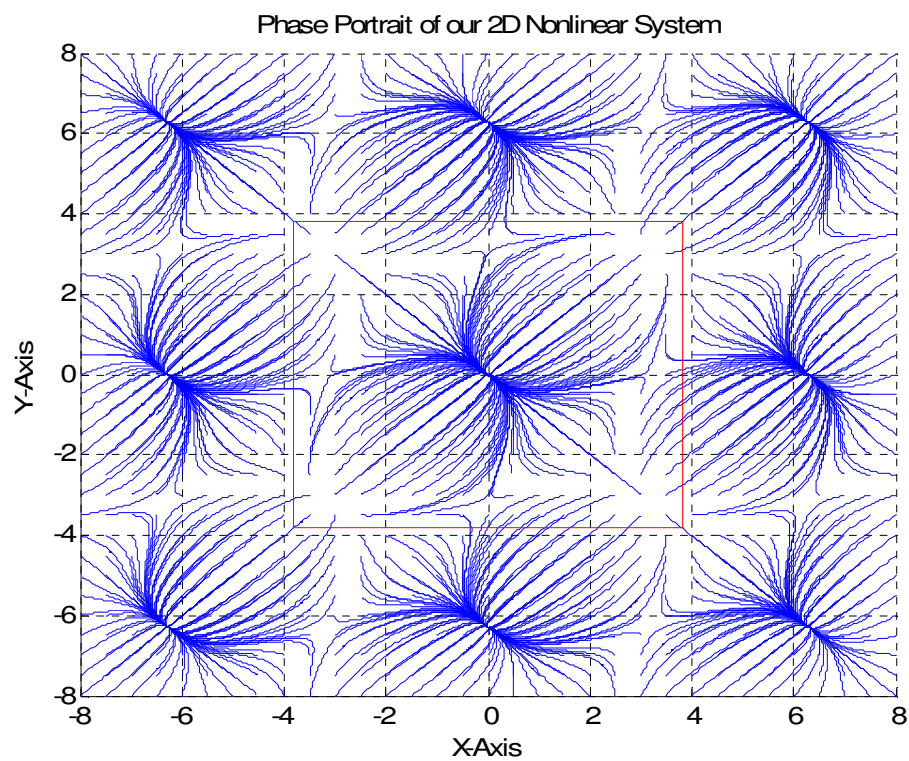


Figure 5.8. Phase Portrait of System II

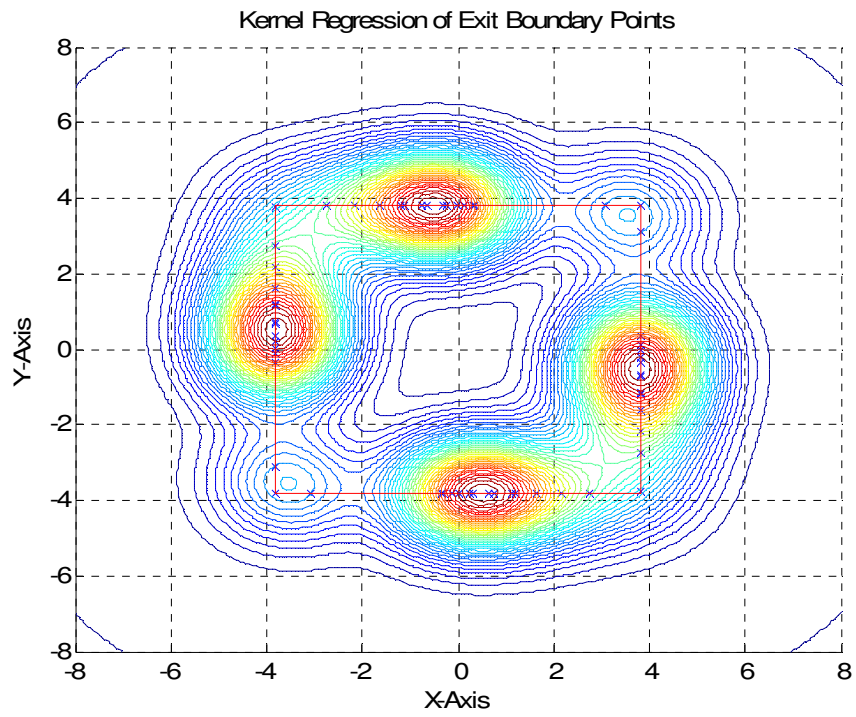


Figure 5.9. Kernel Regression of Exit Boundary Points

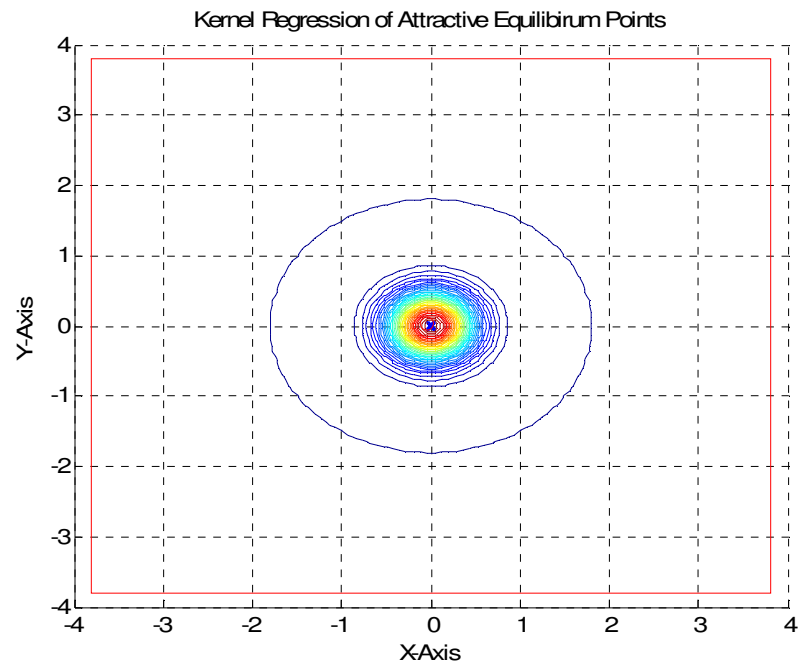


Figure 5.10. Kernel Regression of Attractive Equilibrium Points of System II

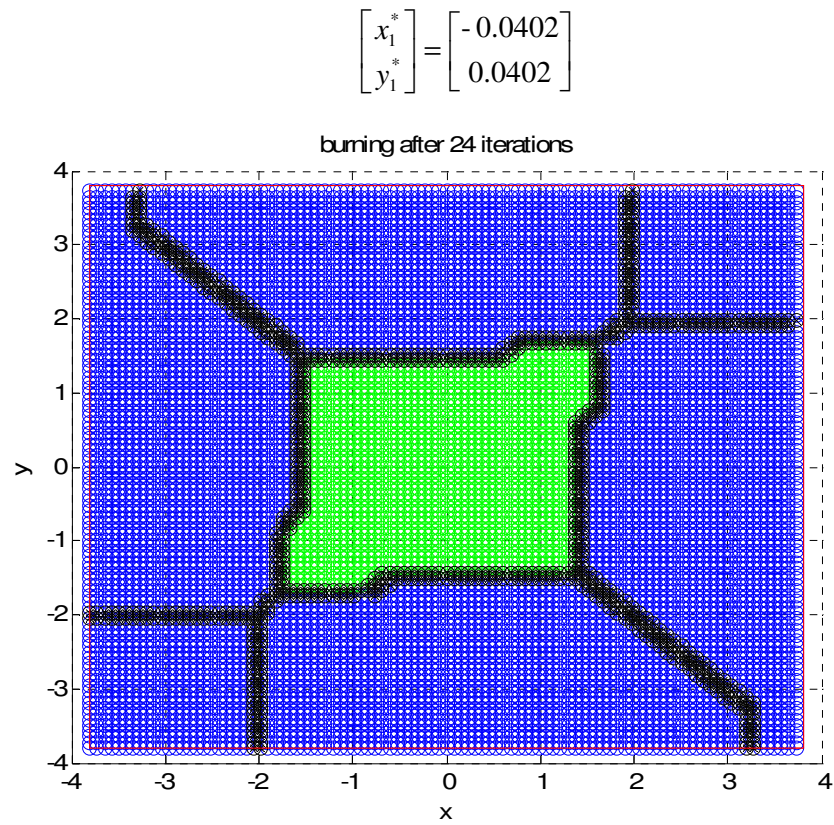


Figure 5.11. System II after Totally Burnt

Border of one of the exit basins:

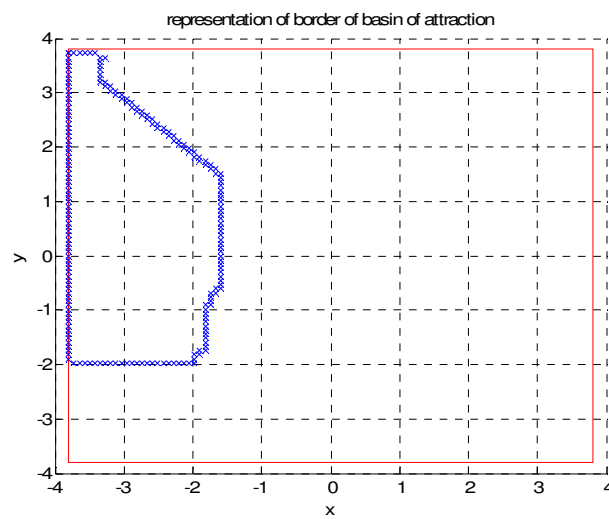


Figure 5.12. Border of one of the Exit Basins of System II

Parametric estimation using 4. model:

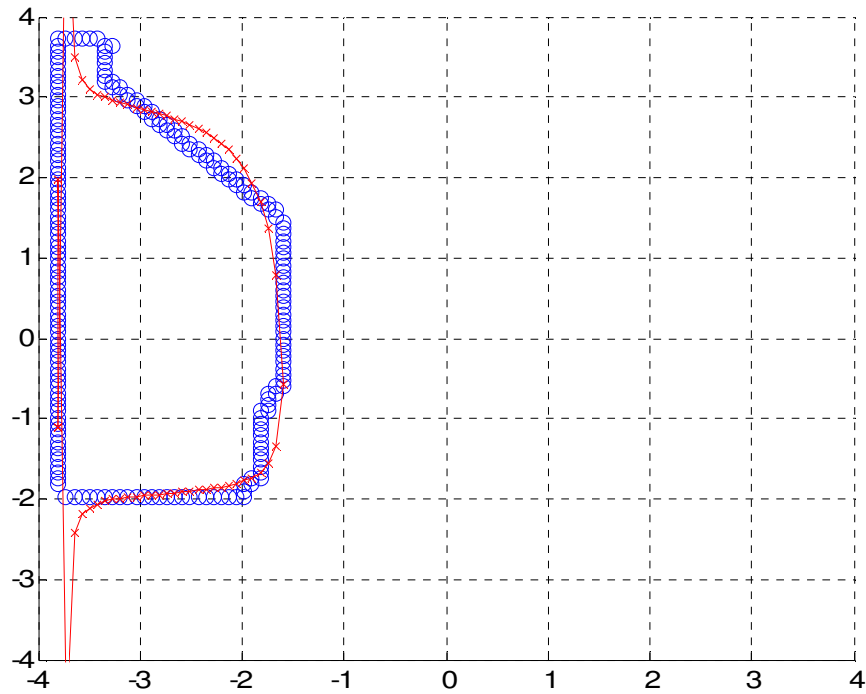


Figure 5.13. Estimation of the Exit Basin of System II

5.3. System III

$$\begin{aligned} \dot{x} &= y & x_0 &= [-8 \quad -7.5 \quad \dots \quad 7.5 \quad 8] \\ \dot{y} &= -(8 + x^2)y + 3x - x^3 & y_0 &= [-8 \quad -7.5 \quad \dots \quad 7.5 \quad 8] \end{aligned}$$

The frame constant n : 4

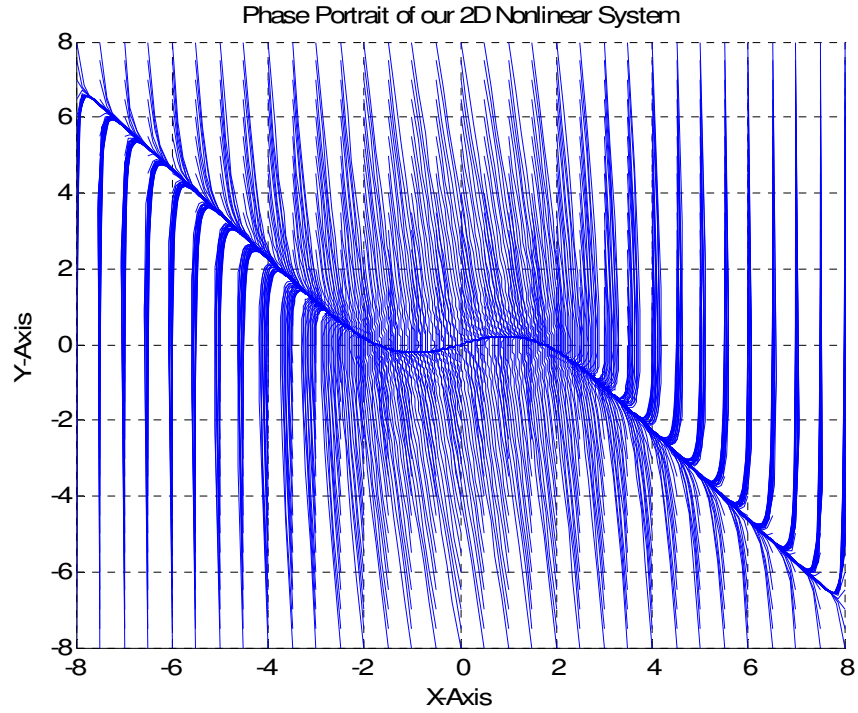


Figure 5.14. Phase Portrait of System III

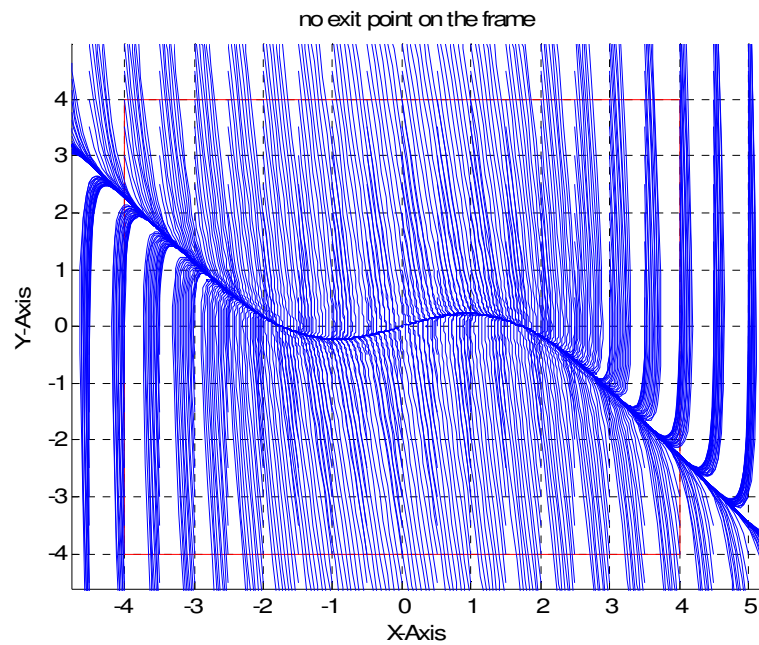


Figure 5.15. Existence of Exit Points of System III

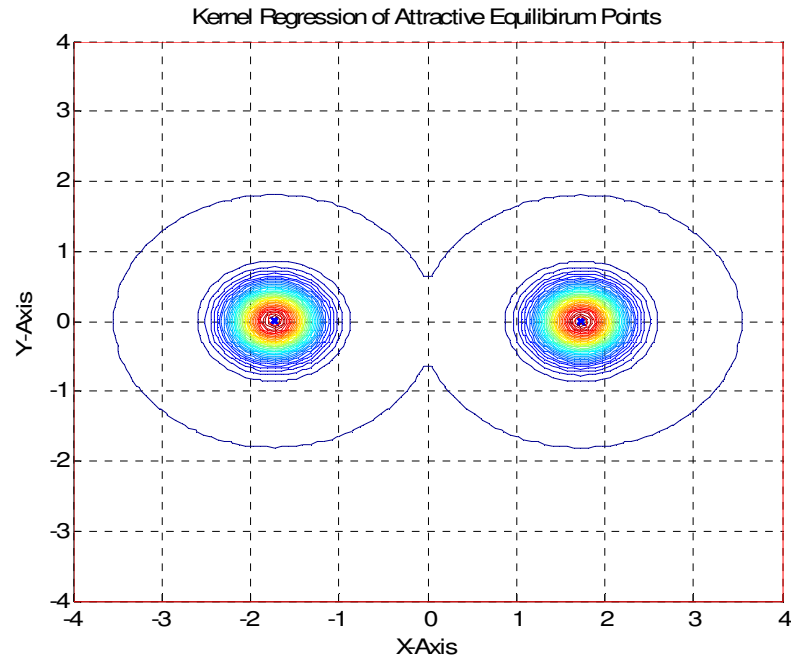


Figure 5.16. Kernel Regression of Attractive Equilibrium Points of System III

$$\begin{bmatrix} x_1^* \\ y_1^* \end{bmatrix} = \begin{bmatrix} 1.7286 \\ -0.0402 \end{bmatrix} \quad \begin{bmatrix} x_2^* \\ y_2^* \end{bmatrix} = \begin{bmatrix} -1.7286 \\ 0.0402 \end{bmatrix}$$



Figure 5.17. Existence of Periodic Orbits of System III

Parametric estimation using 4. model:

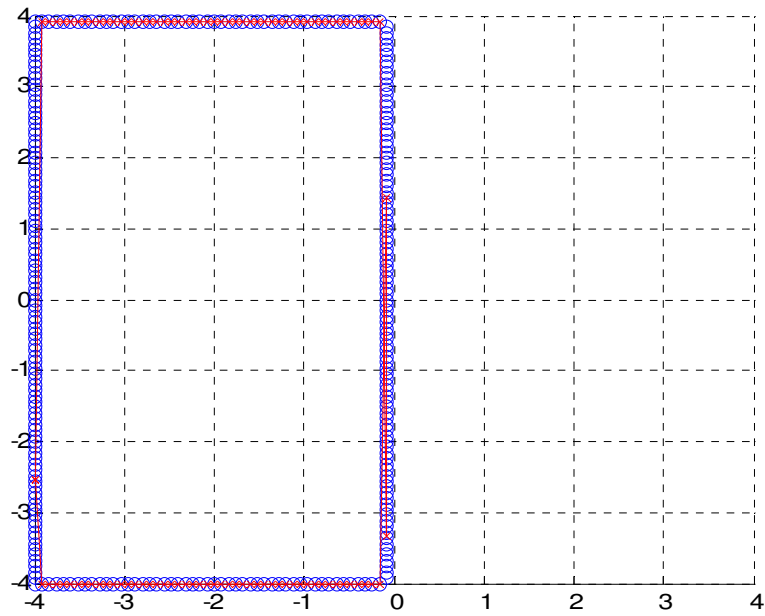


Figure 5.18. Estimation of 1. Basin of Attraction of System III

1. parameter is 0.127264
2. parameter is 0.519236
3. parameter is 0.0407244
4. parameter is 0.0101811
5. parameter is -1.99549
6. parameter is 0.0415389
7. parameter is -8.14162
8. parameter is 0.00325795
9. parameter is -0.638558

Parametric estimation using 3. model:

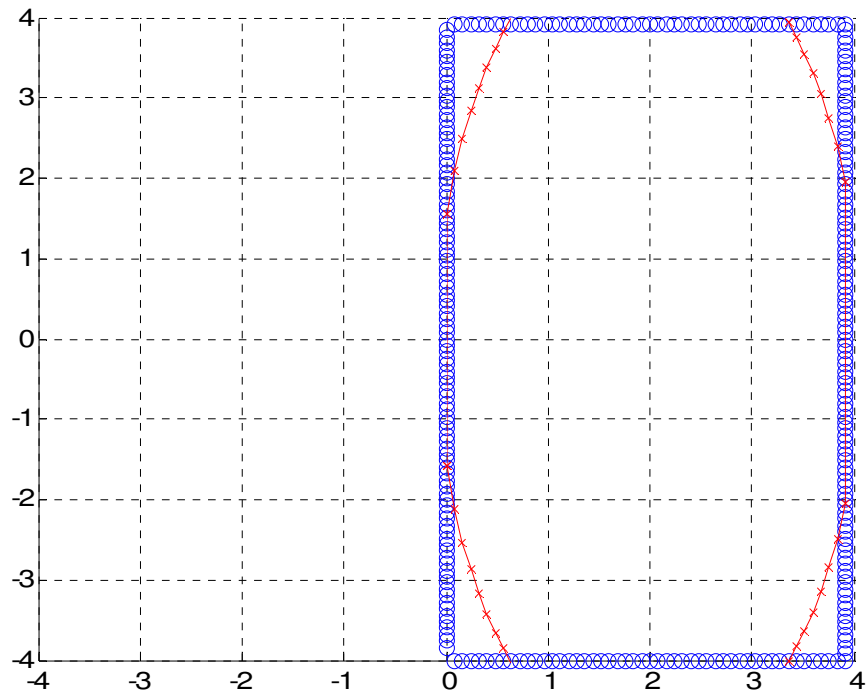


Figure 5.19. Estimation of 2. Basin of Attraction of System III

1. parameter is $7.36636e-028$
2. parameter is $4.70662e-027$
3. parameter is $1.12749e-029$
4. parameter is $-1.87487e-026$
5. parameter is $2.2103e-029$
6. parameter is $-1.79463e-027$

5.4 System IV

$$\dot{x} = 0.5(-h + x^2)$$

$$\dot{y} = 0.2(-x - 1.5y + 1.2)$$

$$h = 17.76x + 103.79x^2 + 229.63x^3 - 226.31x^4 + 83.72x^5$$

$$x_0 = [-0.4 \quad -0.3 \quad \dots \quad 7.9 \quad 8]$$

$$y_0 = [-0.4 \quad -0.3 \quad \dots \quad 7.9 \quad 8]$$

The frame constant $n: 1$

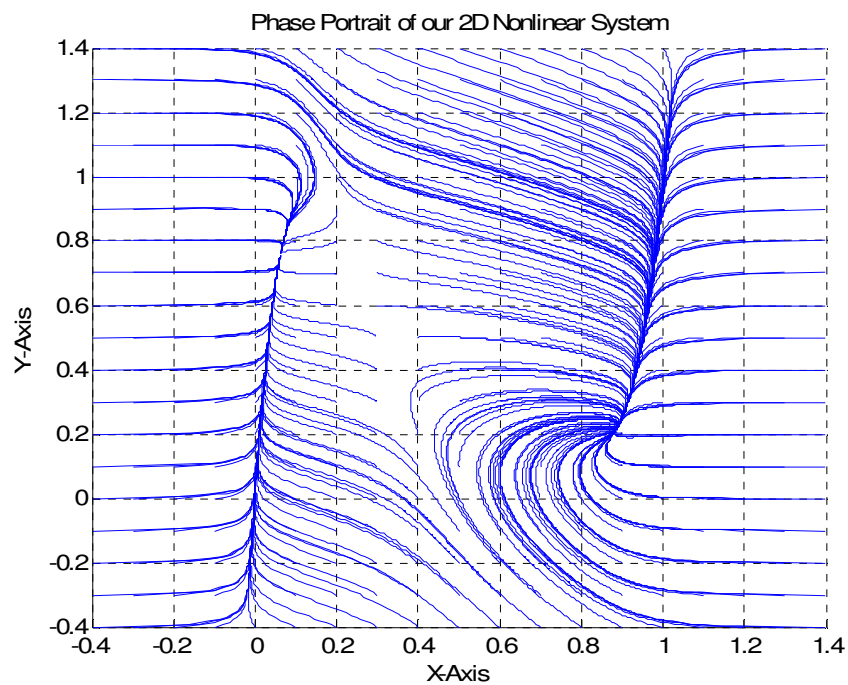


Figure 5.20. Phase Portrait of System IV

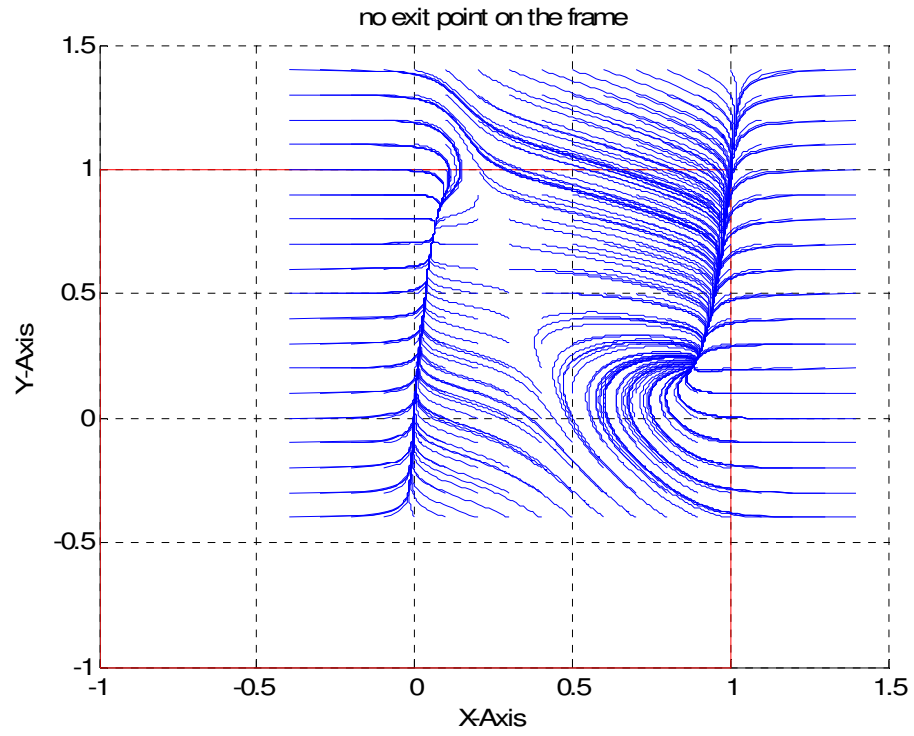


Figure 5.21. Existence of Exit Points of System IV

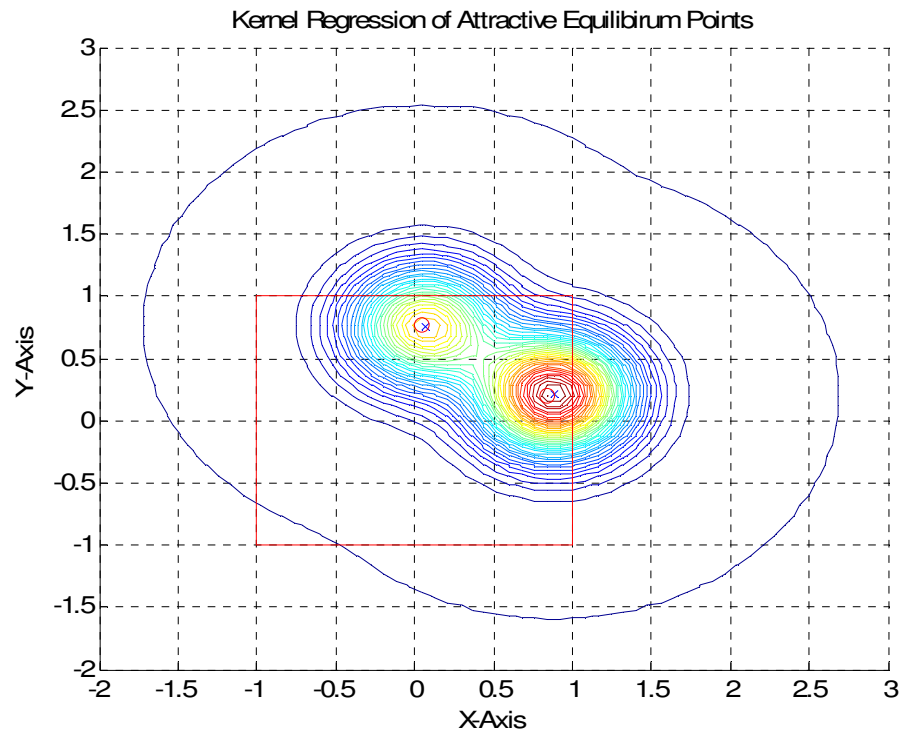


Figure 5.22. Kernel Regression of Attractive Equilibrium Points of System IV

$$\begin{bmatrix} x_1^* \\ y_1^* \end{bmatrix} = \begin{bmatrix} 0.8442 \\ 0.2010 \end{bmatrix} \quad \begin{bmatrix} x_2^* \\ y_2^* \end{bmatrix} = \begin{bmatrix} 0.0402 \\ 0.7638 \end{bmatrix}$$

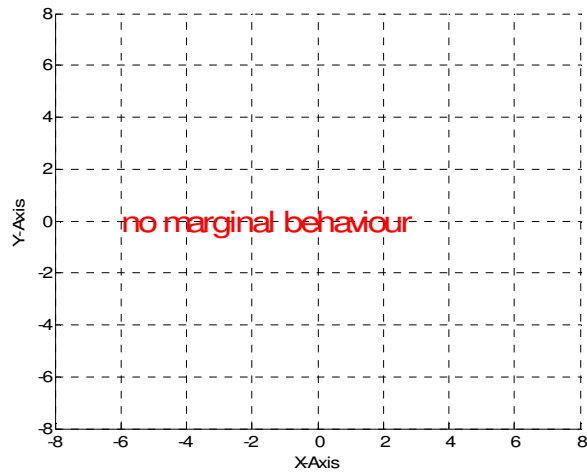


Figure 5.23. Existence of Periodic Orbits of System IV

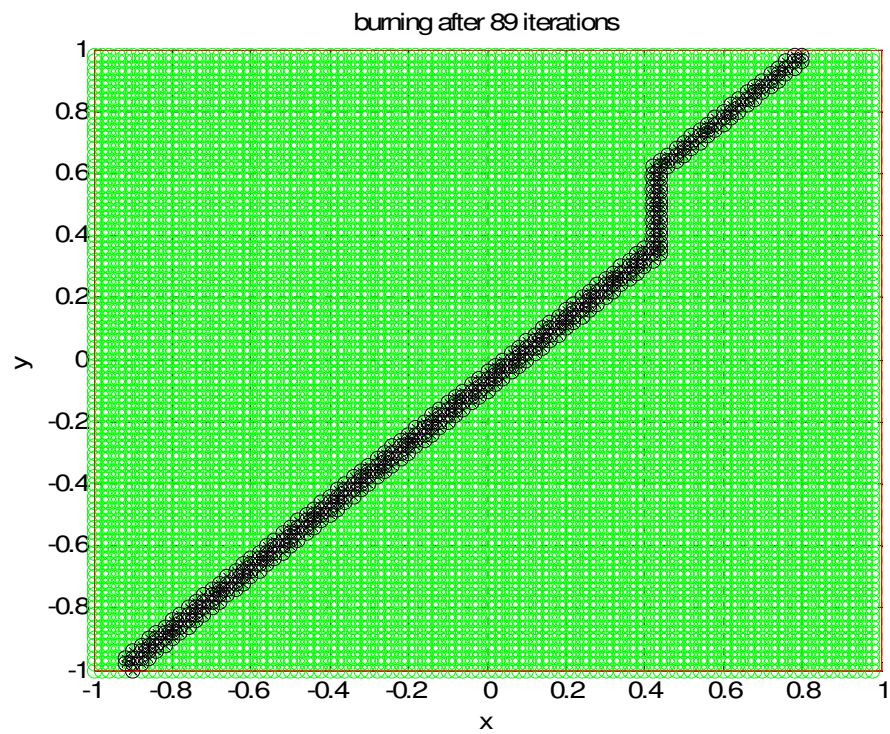


Figure 5.24. System IV after Totally Burnt

Parametric estimation using 4. model

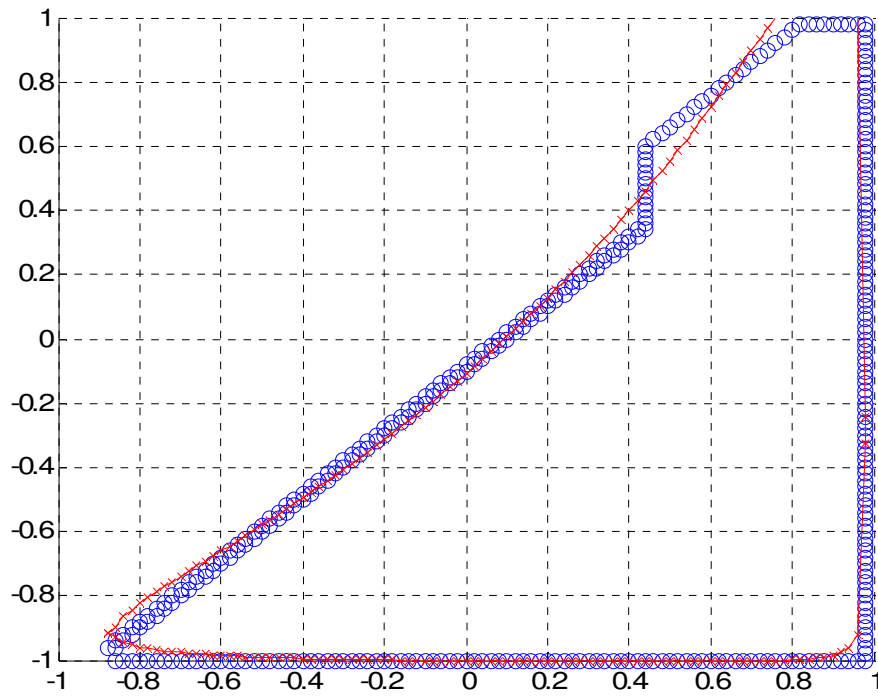


Figure 5.25. Estimation of 1. Basin of Attraction of System IV

1. parameter is 1.07661e-023
2. parameter is -3.98197e-023
3. parameter is 2.89016e-023
4. parameter is 4.38177e-023
5. parameter is 3.35477e-023
6. parameter is -7.55624e-023
7. parameter is -3.60437e-023
8. parameter is 3.20924e-023
9. parameter is 3.12081e-024

Parametric estimation using 2. model

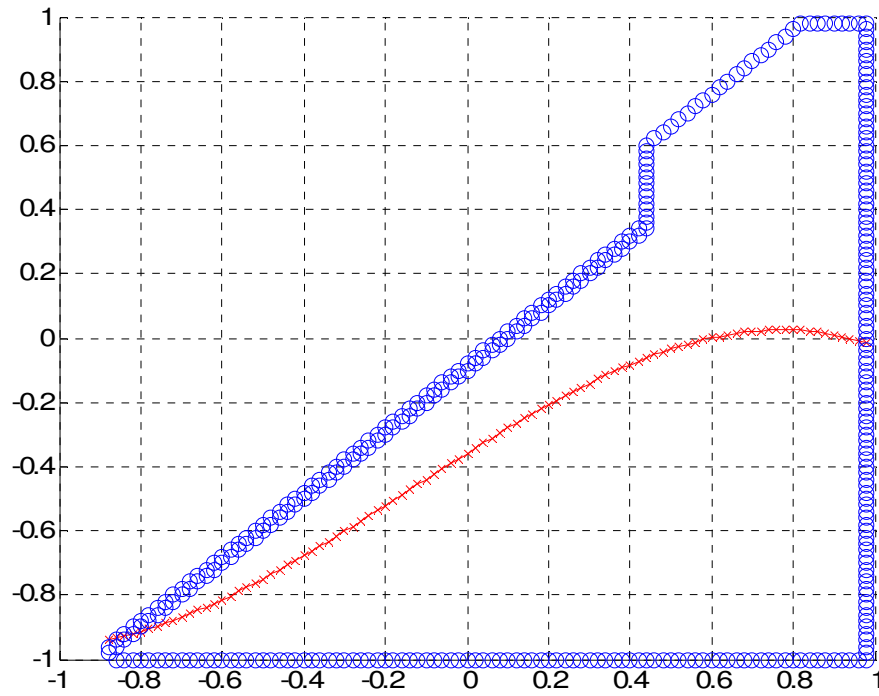


Figure 5.26. Estimation of 1. Basin of Attraction of System IV via Third Order Polynomial

1. parameter is -0.35864
2. parameter is 0.796753
3. parameter is -0.133175
4. parameter is -0.329404

5.5 System V

$$\begin{aligned} \dot{x} &= y - (x^3 - x) & x_0 &= [-8 \quad -7.5 \quad \dots \quad 7.5 \quad 8] \\ \dot{y} &= -x & y_0 &= [-8 \quad -7.5 \quad \dots \quad 7.5 \quad 8] \end{aligned}$$

The frame constant $n=3$

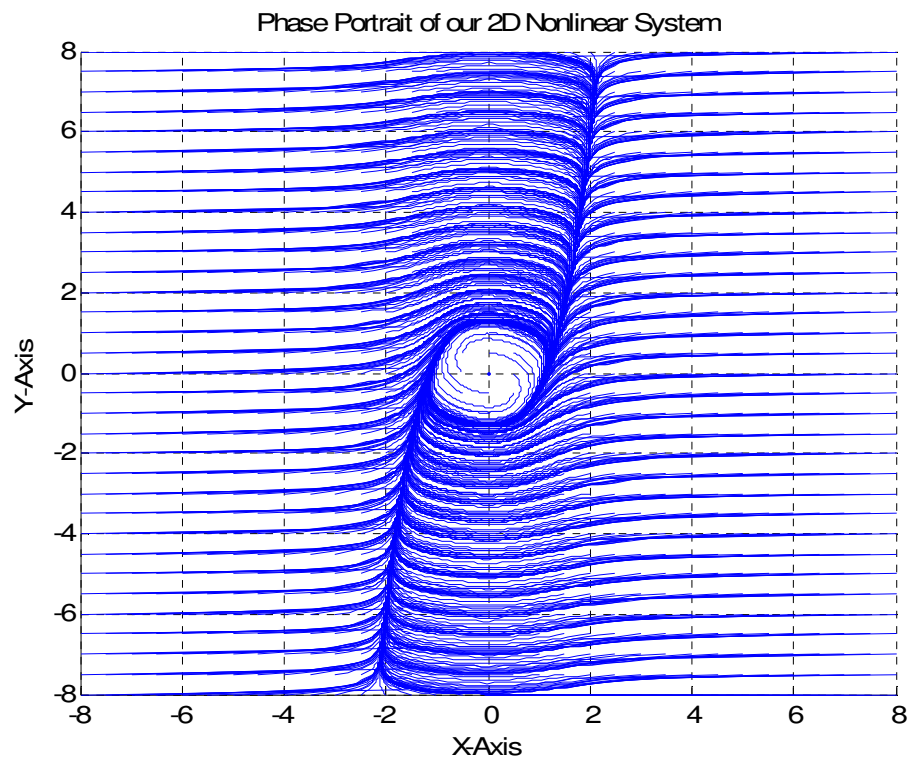


Figure 5.27. Phase Portrait of System V

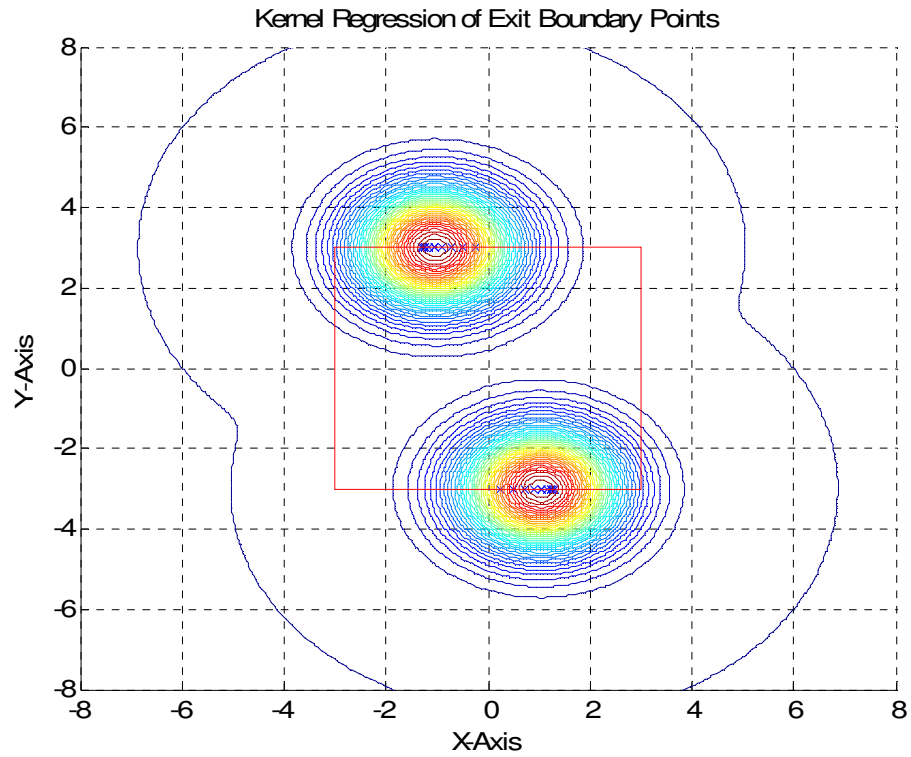


Figure 5.28. Kernel Regression of Exit Boundary Points of System V

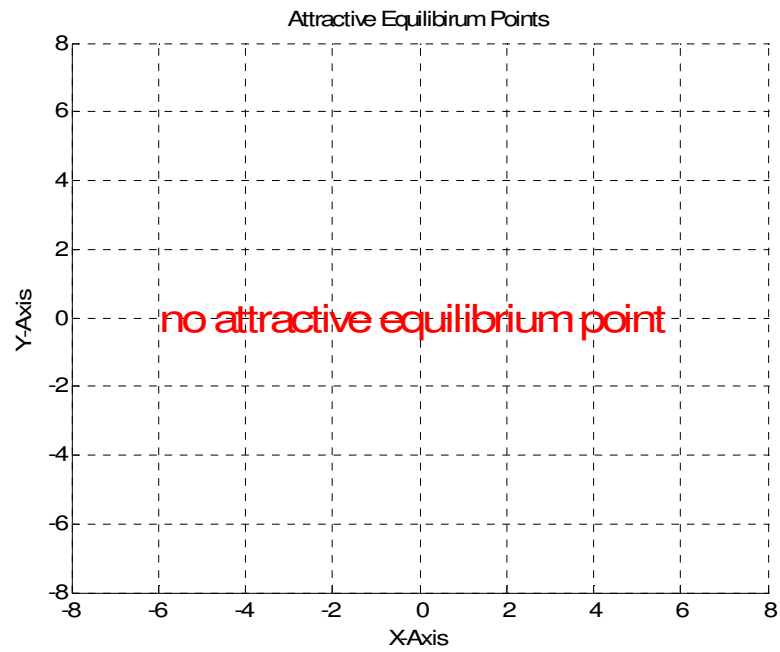


Figure 5.29. Existence of Attractive Equilibrium Points of System V

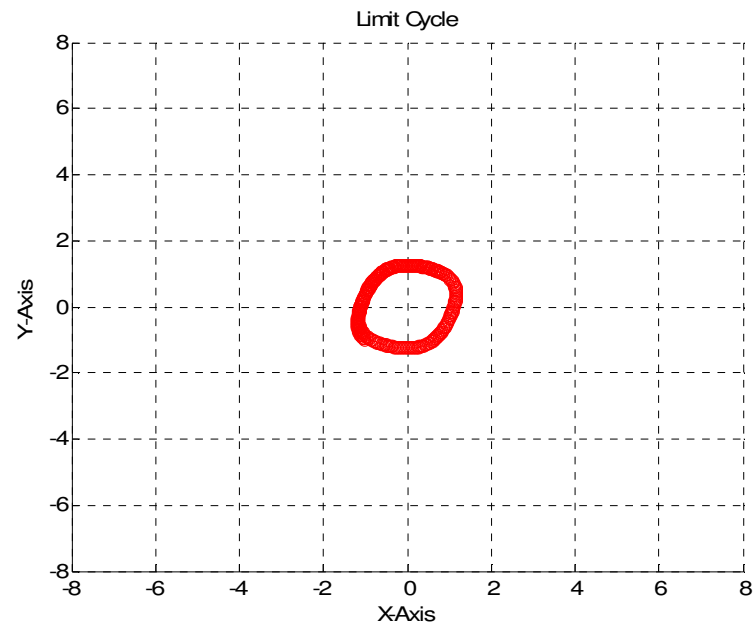


Figure 5.30. Limit Cycle of System V

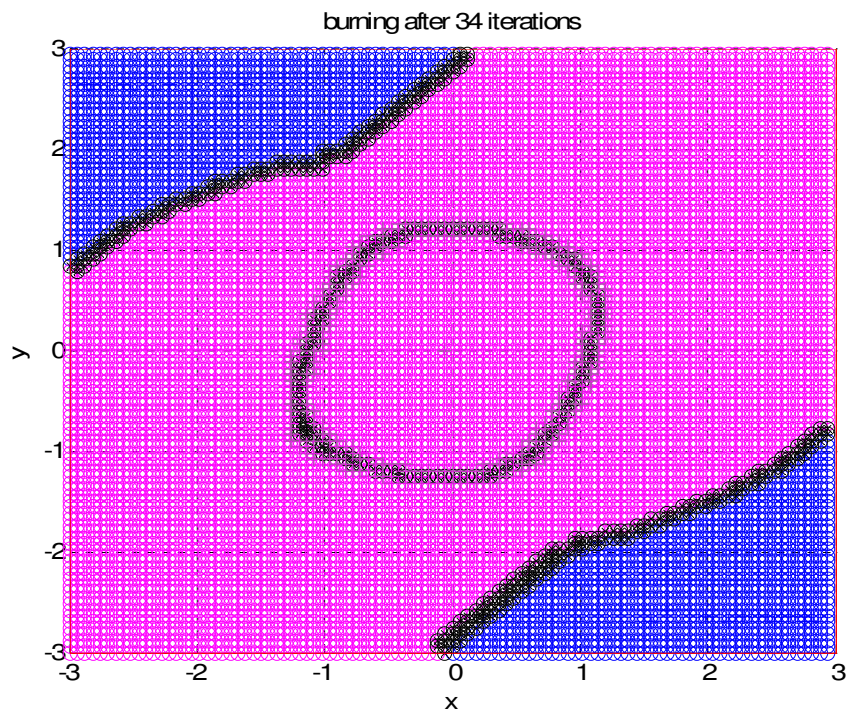


Figure 5.31. System V after Totally Burnt

Parametric regression of the biggest invariant set with 4. model

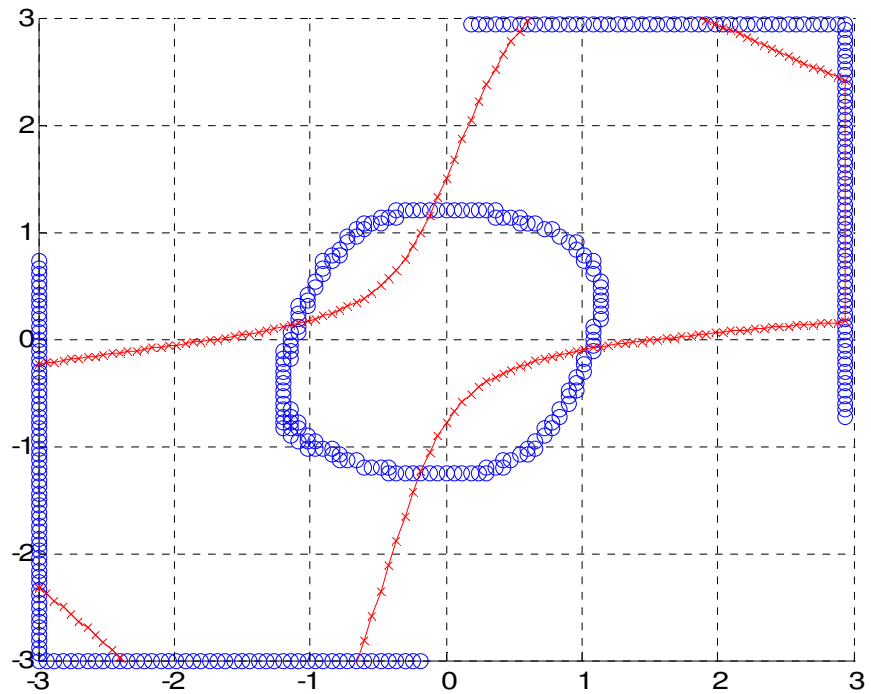


Figure 5.32. Estimation of Basin of Attraction of System V

1. parameter is $9.53908e-027$
2. parameter is $6.63345e-027$
3. parameter is $1.65787e-026$
4. parameter is $-4.34399e-027$
5. parameter is $7.39194e-027$
6. parameter is $-8.71795e-026$
7. parameter is $8.44966e-028$
8. parameter is $-1.17913e-026$
9. parameter is $-1.94238e-026$

Note: For a better fit, a more complicated model should be used.

5.6. Data Point Test

The user is able to test his data point if it is inside the estimated basin boundary.

Example:

For the data point [2 ; 1] , the algorithm checks if

$$ax^2y^2 + bxy^2 + cy^2 + dx^2y + ex^2 + fxy + gx + hy + i < 0$$

where ,

$$a = 9.53908e-027$$

$$b = 6.63345e-027$$

$$c = 1.65787e-026$$

$$d = -4.34399e-027$$

$$e = 7.39194e-027$$

$$f = -8.71795e-026$$

$$g = 8.44966e-028$$

$$h = -1.17913e-026$$

$$i = -1.94238e-026$$

The result is:

$$-1.2369e-025 < 0$$

as expected. Hence the data point is in the basin of the limit cycle.

6. DISCUSSION AND CONCLUSION

Our main aim in this thesis was to find, estimate and represent the basin of invariant sets in a nonlinear system data by using different tools and algorithms. What we have done so far to achieve this aim is summarized below.

Assuming that our sampled nonlinear data satisfies the minimum requirements for our analysis, we searched for 4 types of invariant sets:

- 1- Basin of attraction of stable equilibrium points
- 2- Continuum of periodic orbits
- 3- Basin of attraction of stable limit cycles
- 4- Exit basins, i.e. phase space regions starting from which trajectories leave the region of interest through a connected portion of the boundary hypersurface (in 2d systems this corresponds to boundary line segments)

Multivariable Kernel Regression used almost everywhere in the thesis was the most useful tool in the identification of these invariant sets. After these sets are determined, we introduced our flame expansion algorithm which finds the basin of the invariant sets successfully.

At last we tried to represent the boundaries of the basin of invariant sets via parametric regression.

6.1. Limitations

Most of the limitations of the algorithms developed within realm of the thesis are due to the estimation on basis of finite sampled data. The estimates of steady state behaviour and related basins are limited by the density of initial conditions and sampling frequency of the system trajectories.

Moreover when using Kernel functions and flame expansion algorithm the phase space is covered by a grid. The following type of estimation errors can occur when this grid is not dense enough to reflect the similarities of the underline dynamics:

- Equilibrium Points and small neutral basins may not be distinguished.
- The limit cycles and marginally stable periodic orbits may not be distinguishable.
- The boundaries formed by the flame expansion algorithm may be inaccurate since a small grid size may cause different margins to merge, i.e. in a sparse grid the different equilibrium points can overlap or stay very close to each other so that false boundaries are constructed.

All the estimations along the thesis are highly dependant on the parameters which are chosen by the user. An improper selection of the following parameters may give unexpected results :

- bandwidth matrix for kernel regression
- tolerance value to be used in the detection of periodic orbits
- the step size used in the search of an useful Poincare Line
- more suitable nonlinear models for nonlinear parametric regression

The algorithms in the thesis as shown in examples provide succesful results in 2D systems, they need further development for extension in 3 and higher dimensional systems.

In closed orbit detection, the user should be very careful since the limit cycles and continuum of closed orbits are in most cases very hard to distinguish for the algorithm. When analyzing the closed orbits the user may need to run the program many times with different parameters for the minimum errors.

An additional limitation is for the systems which have more than one continuum of periodic orbits. The algorithm assumes that there is only one continuum of periodic orbits and discards other group of periodic orbits it there is any.

In addition to the limitations mentioned above, the following tasks are open questions to be researched:

- The flame expansion algorithm may be developed so that thinner boundaries are formed.
- The flame expansion algorithm may be changed to circular shaped expansions to prevent the fast expansion in diagonals
- The noise in the data can be removed by using different image processing filters.
- Different shapes for the Kernel Function
- The code can be optimized for a faster execution.

6.2. Future Work

All the parameters in the thesis chosen by the user for the execution of the algorithm can be obtained by a statistical analysis over the system data. If the parameters are selected systematically, they can be more “system-specific” and give more accurate results.

Except improving the overall performance of the program with the suggestions made above, we can focus on 3-dimensional systems with a deeper insight and try to recognize marginal cases, that is to say the continuum of periodic orbits and more complicated behaviours like chaos in these systems. Extensions of devised methods to 3 and higher dimensions.

Development of method for detecting chaotic attractors and their basins of attraction
The basic approach of segmenting of phase space into basins is actually a preliminary work for simplified system description of dynamics of each basin. A natural continuation of this thesis should be the estimation of dynamics within each basin. Preliminary step in this direction have been provided in the additional work.

Actually the work completed in this thesis is meant to be used in an intelligent control algorithm making efficient use of flow dynamics of the system.

A superior final-version of the the program should tell the researcher all the basin of attractions and all the possible invariant sets within their simplified dynamics in any n-dimensional system.

The researcher would ultimately know what will be the fate of his data in future.

REFERENCES

- Arrowsmith, D.K. and C. M. Place , 1994, “*An Introduction to Dynamical Systems*” , Cambridge University Press
- Alligood, K.T. , T.D. Sauer and J.A. Yorke , 2000, “*Chaos, an Introduction to Dynamical Systems*” , Springer Verlag, New York.
- Breiman, L. , W. Mesisel and E. Purcell , 1977, “*Variable Kernel Estimates of Probability Density Estimates*” , Technometrics No.19 , pp. 135-144
- Jones, M.C. , 1990, “*Variable Kernel Density Estimates and Variable Kernel Density Estimates*” , The Australian Journal of Statistics No. 32, pp.361-371
- Lasota, A. and M.C. Mackey, 1991, “*Chaos, Fractals and Noise*” , Springer Verlag, New York
- Parzen, E., 1962, “*On Estimation of Probability Density Function and Mode*” , The Annals of Mathematical Statistics, Vol. 33, No.3, pp.1065-1076
- Perko, L., 1991, “*Differential Equations and Dynamical Systems*” , Springer Verlag, New York
- Scott, D.W. ,1992, “*Multivariate Density Estimation; Theory, Practice and Visualization*”, Wiley-Interscience, New York
- Slotine, J.J. and W. Li, 1990, “*Applied Nonlinear Control*” , Prentice Hall
- Strogatz, S.H. , 2000, “*Nonlinear Dynamics and Chaos*”, Perseus Publishing, Cambridge
- Terrell, G.R. and D.W. Scott, 1992, “*Variable Kernel Density Estimation*” , The Annals of Statistics No.20, p.p.1236-1265

Wand M.P. and M.C. Jones , 1994, "*Kernel Smoothing*" , Chapman & Hall, New York

Wiggins S., 1990, "*Introduction to Applied Nonlinear Dynamical Systems and Chaos ,
Systems*" , Springer Verlag, New York